Relativistic Model for Electroproduction of Nucleon Resonances. II*

P. L. PRITCHETT,† J. D. WALECKA, AND P. A. ZUCKER†
Institute of Theoretical Physics, Department of Physics, Stanford University, Stanford, California 94305
(Received 14 March 1969)

A relativistic gauge-invariant model for electron excitation of nucleon resonances introduced previously is developed and extended. A coupled-channel calculation is carried out retaining the $|\pi N\rangle$ and $|\pi N^*(1236)\rangle$ channels and assuming that one eigenphase shift is resonant. The eigenphase shift is determined from phase-shift analyses of π-N scattering, and the mixing angle from the decay widths of the resonance. The model chosen for the resonant amplitude is a product of two factors: a generalized Feynman amplitude for excitation of the resonant channel, and a final-state enhancement factor which is related to an integral over the eigenphase shift. The model is shown to be an approximate solution to the coupled-channel Omnès equations. Further extensions consist of including $N^*(1236)$ exchange in the excitation amplitude for the $|\pi N\rangle$ channel and of investigating the effect of different fits to G_{En} on the inelastic form factors. The predictions of the theory are compared with all existing data—in particular, with the recent results from SLAC.

1. INTRODUCTION

ELECTRON scattering provides a powerful tool for studying the structure of the nucleon. Electrons interact only electromagnetically with the local current density in the target, and therefore the interaction, in addition to being known, is relatively weak and does not greatly disturb the structure of the target. In addition, for a fixed-energy transfer, one can vary the four-momentum transferred to the target and thus map out the Fourier transform of the transition current density. With the advent of very-high-energy electron accelerators, for example, the Cambridge Electron Accelerator (CEA), the Deutsches Electron Synchrotron (DESY), and especially the Stanford Electron Accelerator (SLAC), electron excitation has become a practical means for studying the details of the excited states of the nucleon.

If only the final electron is detected, as is the case in the SLAC experiments, one can show on general grounds that the cross section for electron excitation of a nucleon isobar of mass W_R is given by[1]

$$\left(\frac{d\sigma}{d\Omega_2}\right)_{\text{lab}}=\frac{\alpha^2\cos^2(\tfrac{1}{2}\theta)}{4\epsilon_1^2\sin^4(\tfrac{1}{2}\theta)[1+(2\epsilon_1/m)\sin^2(\tfrac{1}{2}\theta)]}\times\{(k^4/k^{*4})|f_c|^2+[k^2/2k^{*2}+(W_R^2/m^2)\tan^2(\tfrac{1}{2}\theta)]\times[|f_+|^2+|f_-|^2]\}. \quad (1.1)$$

In this expression, ϵ_1 is the incident electron energy, θ is the electron scattering angle, m is the nucleon mass, k^2 is the invariant four-momentum transferred to the target, and k^* is the proton three-momentum in the isobar rest frame. The Coulomb and transverse form factors $|f_c|^2$ and $|f_+|^2+|f_-|^2$ are functions of k^2. This formula is the inelastic analog of the Rosenbluth cross section. Just as in the elastic case, the two form factors can be separated by making a straight-line plot against $\tan^2(\frac{1}{2}\theta)$ at fixed k^2 and energy loss or by working at $\theta=\pi$, where there is only a transverse contribution. The transverse contribution can also be obtained at one point, $k^2=0$, from the integrated photoabsorption cross section

$$\int_{\text{lab; over resonance}}\sigma_\gamma(\omega)d\omega=[4\pi^2\alpha W_R^2/m(W_R^2-m^2)]\times(|f_+|^2+|f_-|^2)_{k^2=0}. \quad (1.2)$$

The threshold behaviors of the form factors in the variable k^* can also be given on general grounds.[1]

Because quantitative dynamical calculations of the properties of the nucleon resonances are not yet possible, one is forced to work with models. In a previous paper[2] (hereafter referred to as I) a very simple model was presented in order to get a qualitative understanding of the behavior of the inelastic form factors. The basic idea is to view the isobar as a resonance in pion electroproduction, and to write for the resonant multipoles an expression of the form

$$a(W,k^2)=a^{\text{lhs}}(W,k^2)/D(W), \quad (1.3)$$

where W is the total energy in the c.m. system of the pion and nucleon. In this expression $a^{\text{lhs}}(W,k^2)$ is the multipole projection of a gauge-invariant set of Feynman graphs which are thought to play an important role in the excitation process, and $D(W)$ is a final-state enhancement factor which provides the resonance mechanism. For example, in the elastic case there is an expression due to Watson,[3]

$$D(W)=\exp\left(-\frac{1}{\pi}\int_{W_0}^{\infty}dW'\frac{\delta(W')}{W'-W-i\epsilon}\right), \quad (1.4)$$

where δ is the π-N phase shift in the appropriate channel. The approximation of Eq. (1.3) is not restricted to the elastic case, however, and the possibility of inelastic

* Research sponsored by the Air Force Office of Scientific Research, Office of Aerospace Research, U. S. Air Force, under AFOSR Contract No. F44620-68-C-0075.
† National Science Foundation Predoctoral Fellow.
[1] J. D. Bjorken and J. D. Walecka, Ann. Phys. (N. Y.) 38, 35 (1966).
[2] J. D. Walecka and P. A. Zucker, Phys. Rev. 167, 1479 (1968). See this paper for references to previous work.
[3] K. M. Watson, Phys. Rev. 88, 1163 (1952).

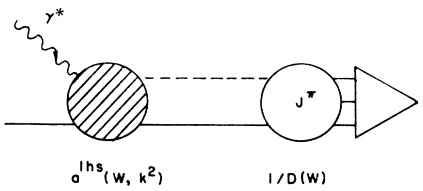

FIG. 1. Model for electroproduction of nucleon resonances.

decay of the resonance is easily taken into account by multiplying the pion electroproduction resonant cross section by a factor $\Gamma_{\rm tot}(W)/\Gamma_{\rm el}(W)$, the ratio of the total to the elastic widths. The model and its theoretical justification are discussed in Sec. 2. It has the advantage of keeping all the general properties of the theory such as Lorentz covariance, current conservation and gauge invariance, threshold behaviors, analyticity, and the final-state theorem (in the elastic case). In I, expressions were given for the inelastic form factors keeping π, ω, and N exchange as the important excitation mechanisms. The over-all contribution of the ω^0 exchange graph was treated as a single parameter, and a fit to all the existing inelastic electron scattering data was obtained for a value of this parameter in reasonable agreement with other determinations of this quantity.[4] The over-all normalization constant for each resonance region was treated as a free parameter and the relative strengths of the various resonances were normalized to their contributions in photoproduction as determined from phenomenological analyses of this process. This calculation shall be referred to as model I.

In the present paper, this model has been developed and extended. The content of Eq. (1.3) can be viewed pictorially, as indicated in Fig. 1. One first produces the $|\pi N\rangle$ system in the state J^π with an amplitude $a^{\rm lhs}(W,k^2)$ and then, through rescattering, a resonance is built up which is allowed to decay into any of the available channels. If a resonance decays strongly into inelastic channels, however, one must also include the formation of the resonance through these inelastic channels. This has been done by making a simple model of the inelasticities, and the model, together with its theoretical justification, is discussed in Sec. 3. The basic idea is to assume that only two strong interaction channels are important, and that only one particular linear combination, or one eigenchannel, is resonant. It is then assumed for simplicity that the other eigenphase shift is small. In this case, the scattering amplitude in the elastic channel (which we denote by $|1\rangle$) is given by

$$(e^{2i\delta_1}-1)/2i=(\cos^2\varepsilon)e^{i\xi}\sin\xi\,, \tag{1.5}$$

where ε is the mixing angle and ξ is the eigenphase shift. Also, at resonance, the partial widths for decay into the two available channels are then directly related to the mixing angle by

$$\Gamma_1/\Gamma=\cos^2\varepsilon\,, \tag{1.6}$$

$$\Gamma_2/\Gamma=\sin^2\varepsilon. \tag{1.7}$$

Because it is now the state

$$|e\rangle=\cos\varepsilon|1\rangle+\sin\varepsilon|2\rangle, \tag{1.8}$$

which can rescatter and resonate once it is produced, one can easily extend the ideas of Eq. (1.3) and write for the multipole amplitudes for excitation of the resonant state

$$a(W,k^2)=[a_1{}^{\rm lhs}(W,k^2)\cos\varepsilon + a_2{}^{\rm lhs}(W,k^2)\sin\varepsilon]/D(W), \tag{1.9}$$

where $D(W)$ is now related to the *real eigenphase shift* by

$$D(W)=\exp\left(-\frac{1}{\pi}\int_{W_0}^{\infty}dW'\frac{\xi(W')}{W'-W-i\epsilon}\right). \tag{1.10}$$

The eigenphase shift and mixing angle determined from Eq. (1.5) in this two-channel analysis are discussed in Sec. 4, as is the corresponding determination of $D(W)$ from Eq. (1.10). There is one further complication in that there are already experimental indications as well as theoretical reasons for believing that

$$\xi(W)\xrightarrow[W\to\infty]{}\tfrac{1}{2}\pi \tag{1.11}$$

for these resonant states. This yields a fully absorptive amplitude at high energy. In this case one is forced to make a subtraction in the expression for $D(W)$ and write

$$D(W)=\exp\left(-\frac{(W-M_s)}{\pi}\times\int_{W_0}^{\infty}\frac{\xi(W')dW'}{(W'-M_s)(W'-W-i\epsilon)}\right),$$

$$D(M_s)=1.$$

Therefore, there is still one free parameter M_s, or the over-all strength for each resonance, and again the contribution of each resonance has to be normalized to the value known from photoproduction.[5] One can, however, ask whether the values obtained for the subtraction point M_s are in qualitative accord with an understanding of the strong-interaction dynamics, and this is discussed in the summary. The model then allows a computation not only of the form factors for

[4] In I, two fits were actually found depending on the sign of $g_{\omega\pi\gamma}g_{\omega NN}$. In the high-$l$-dominant case, the highest spin resonances $\frac{3}{2}^+$ (1236), $\frac{3}{2}^-$ (1525), $\frac{5}{2}^-$ (1680), $\frac{5}{2}^+$ (1688), and $\frac{7}{2}^+$ (1950) dominated the inelastic spectrum and the contributions of the s-wave resonances which also lie in these regions were negligible. In the second, or s-wave-dominant case, just the opposite occurred and as soon as $k^2\neq 0$, the $\frac{1}{2}^-$ (1550), $\frac{1}{2}^-$ (1640), and $\frac{1}{2}^-$ (1710) made the major contribution to the inelastic cross section. The model is poorest for s waves, however, and the results of the present paper would tend to favor the high-l-dominant case. One cannot really decide this issue until the multipolarity of the transition form factors are determined as a function of k^2. This will require coincidence experiments.

[5] It is clear from Eq. (1.5) that the *sign* of ε must also still be chosen for each resonance.

the resonances, but also of the resonant spectrum and shapes of the resonances as a function of W. This is discussed in Sec. 4.

In discussing the higher nucleon resonances the two channels $|\pi N\rangle$ and $|\pi N^*(1236)\rangle$ have been kept. In the latter case there are two helicity amplitudes for a given J^π, and just that combination corresponding to the lowest l value in the $|\pi N^*\rangle$ system has been included. It is assumed that all the inelastic decays of the higher resonances into $|\pi\pi N\rangle$ go through the $|\pi N^*(1236)\rangle$ channel in order to get some insight into the qualitative effects of the inelasticities. As an excitation mechanism for the $|\pi N^*(1236)\rangle$ channel, π, N, and the convection current part (for current conservation) of N^* exchange have been kept. ω^0 exchange is ruled out by isospin. The coupling constants in this amplitude are all known. Section 5 contains a discussion of this amplitude and its multipole projections, and the results are compared with the predictions of model I. The results are also compared with the general threshold predictions.[1]

In Sec. 6 modifications and improvements of the model are discussed. In particular, the effects of varying the elastic form factors which enter through the excitation mechanism and of including $N^*(1236)$ exchange in the excitation amplitude for the $|\pi N\rangle$ channel are investigated.

In Sec. 7 the theoretical results are compared with all the existing data on the $N(ee')N^*$ form factors and with the new experimental results from SLAC.[6] Section 8 contains a summary and the conclusions.

The general coincidence cross section is discussed in Appendix C.

2. REVIEW OF THE MODEL

In this section the model developed in I is reviewed. The first step is to make a general covariant analysis of the transition matrix element for the process

$$\gamma^*+N\rightarrow N+\pi, \tag{2.1}$$

where γ^* is the Møller potential from the electron. There are six independent kinematic invariants which can be chosen to be explicitly gauge-invariant, that is, replacing $\epsilon_\mu\rightarrow k_\mu$ gives identically zero. These are multiplied by six invariant amplitudes which are functions of three scalar variables. In the center-of-momentum frame for the above process these invariant amplitudes can be expressed in terms of the independent electromagnetic transition multipoles: transverse electric and magnetic multipoles and a Coulomb multipole for each value of J^π of the final state.[7] At this stage, whatever approximation is put in for the individual multipoles, the over-all amplitude remains gauge-invariant and covariant. The above results, together with the formulas for projecting a given multipole from a gauge-invariant set of Feynman graphs for pion electroproduction, are presented in detail in I and will not be repeated here. Let us consider, then, the resonant multipole amplitudes.

Suppose one has solved the problem of π-N scattering and has the solution for the partial-wave amplitude (labeled by $l^\pm$) in the form

$$f=(e^{i\delta}\sin\delta)/q=N(W)/D(W), \tag{2.2}$$

where $N(W)$ has only left-hand singularities and is real for $W>m+\mu$. If the problem has been solved correctly, resonances will be found in the appropriate partial-wave amplitudes. A resonance can be defined as the place where

$$\mathrm{Re}D(W_R)=0, \tag{2.3}$$

and in the vicinity of the resonance $D(W)$ can be expanded as

$$D(W)\cong(W-W_R)[(d/dW)\,\mathrm{Re}D(W)]_{W=W_R}+i\,\mathrm{Im}D(W_R), \tag{2.4}$$

$$D(W)=\mathrm{Re}'D(W_R)[W-W_R+\tfrac{1}{2}i\Gamma]. \tag{2.5}$$

It then follows that

$$f=(e^{i\delta}\sin\delta)/q\cong-\Gamma_{\mathrm{el}}/2q(W-W_R+\tfrac{1}{2}i\Gamma), \tag{2.6}$$

where use has been made of the general unitarity condition

$$\mathrm{Im}(1/f)=-q\sigma_{\mathrm{tot}}/\sigma_{\mathrm{el}}=-q\Gamma/\Gamma_{\mathrm{el}}. \tag{2.7}$$

σ_{tot} and σ_{el} are the total and elastic cross sections in the $l^\pm$ channel.[8] The model now consists of taking the following expression as an approximate electroproduction multipole amplitude in the vicinity of a resonance in the $l^\pm$ channel:

$$a(W,k^2)\cong a^{\mathrm{lhs}}(W,k^2)[(e^{i\delta}\sin\delta)/qN(W)], \tag{2.8}$$

$$a(W,k^2)=a^{\mathrm{lhs}}(W,k^2)/D(W), \tag{2.9}$$

where $a^{\mathrm{lhs}}(W,k^2)$ stands for the multipole projection

[6] E. Bloom, D. Coward, H. DeStaebler, J. Drees, J. Litt, G. Miller, L. Mo, R. E. Taylor, M. Breidenbach, J. I. Freidman, H. W. Kendall, and S. Loken, SLAC Group A, reported by W. K. Panofsky in *International Conference on High-Energy Physics, Vienna, 1968* (CERN, Geneva, 1968), p. 23.

[7] There is only one transverse multipole for $J=\frac{1}{2}$ states.

[8] This discussion has for simplicity neglected any nonresonant background. Suppose that

$$\delta=\delta_R+\delta_b,$$

where δ_R is the resonant phase shift and δ_b is real, representing an elastic background. Then

$$|f|^2=|(e^{2i\delta}-1)/2iq|^2=|f_R+f_b^*|^2,$$

where

$$f_R=(e^{2i\delta_R}-1)/2iq$$

is the resonant part of the amplitude. Then $\mathrm{Im}\delta_R\geq 0$ by unitarity and

$$\mathrm{Im}(1/f_R)=-q\sigma_{\mathrm{tot}}{}^R/\sigma_{\mathrm{el}}{}^R$$

in terms of the resonant cross section. Writing

$$f_R=N_R(W)/D_R(W),$$

the discussion can be carried through using just the resonant quantities.

of any gauge-invariant set of exchange graphs that are thought to play an important role as an excitation mechanism. This approximation has the following features to recommend it: (i) It has the correct singularity structure since $a^{\rm lhs}(W,k^2)$ has the appropriate left-hand singularities in W, and $D(W)$ has the physical right-hand cut.[9] (ii) It has built into it the correct threshold behaviors in both k^* and q. (iii) It satisfies the final-state theorem in the region of elastic scattering since there

$$D(W)=|D(W)|e^{-i\delta}. \tag{2.10}$$

(iv) It is a solution to the Omnès equation for the multipole amplitude in the elastic case provided only that $a^{\rm lhs}(W,k^2)$ is a slowly varying function of W in the region where $\sin\delta\neq 0$. *Note that the approximation is not restricted to the elastic region, however.* (v) The electroproduction amplitude then resonates at the same place as the scattering amplitude.

To see this, use Eq. (2.5) and write

$$a(W,k^2)\cong a^{\rm lhs}(W_R,k^2)/[{\rm Re}'D(W_R)(W-W_R+\tfrac{1}{2}i\Gamma)]. \tag{2.11}$$

The pion electroproduction cross section integrated over a resonance peak, which has a direct interpretation in terms of the inelastic form factors $|f_c|^2$ and $|f_+|^2+|f_-|^2$, is then

$$\int_{\rm Res} dW\,|a(W,k^2)|^2{}_{\gamma^*+N\to N+\pi}=\frac{2\pi}{\Gamma}\left|\frac{a^{\rm lhs}(W_R,k^2)}{{\rm Re}'D(W_R)}\right|^2. \tag{2.12}$$

Clearly, if there are inelastic processes present and only the electron is observed, one must sum over these processes. The result is to multiply the above by $\Gamma/\Gamma_{\rm el}=\sigma_{\rm tot}/\sigma_{\rm el}$ and therefore

$$\int_{\rm Res} dW\,|a(W,k^2)|^2{}_{\gamma^*+N\to N+\text{anything}}=\frac{2\pi}{\Gamma}\frac{\sigma_{\rm tot}}{\sigma_{\rm el}}\left|\frac{a^{\rm lhs}(W_R,k^2)}{{\rm Re}'D(W_R)}\right|^2. \tag{2.13}$$

Note that this model provides an analytic expression for the k^2 dependence of the inelastic form factors through the function $|a^{\rm lhs}(W_R,k^2)|^2$.

In I, two theoretical derivations of this model were presented. Only one of them is reviewed here, the result quoted in (iv), since it will be relevant to the discussion in the next section and provides an explicit representation of $D(W)$. This discussion here is confined to the elastic case for simplicity.

[9] The numerator in Eq. (2.9) is not subject to the uncertainties of integrations over left-hand cuts and the frequently attendent cutoffs that are necessary. The present approach, however, provides just a model of the left-hand region.

For the electroproduction amplitude, one really has an Omnès equation to solve of the type

$$a(\omega,k^2)=a^{\rm lhs}(\omega,k^2)+\frac{1}{\pi}\int_1^\infty \frac{h^*(\omega')a(\omega',k^2)d\omega'}{\omega'-\omega-i\epsilon}, \tag{2.14}$$

where

$$h(\omega)=e^{i\delta(\omega)}\sin\delta(\omega), \tag{2.15}$$

and

$$\delta(\infty)=0, \tag{2.16}$$

$$\delta(1)=n\pi, \tag{2.17}$$

where n is the number of bound states in the particular channel. This singular integral equation was solved exactly by Omnès, and the solution is[10]

$$a(\omega,k^2)=e^{i\delta(\omega)}\left[a^{\rm lhs}(\omega,k^2)\cos\delta(\omega)+e^{\rho(\omega)}\frac{\mathcal{P}}{\pi}\times\int_1^\infty\frac{a^{\rm lhs}(\xi,k^2)\sin\delta(\xi)e^{-\rho(\xi)}d\xi}{\xi-\omega}\right], \tag{2.18}$$

where

$$\rho(\omega)=\frac{1}{\pi}\mathcal{P}\int_1^\infty d\zeta\frac{\delta(\zeta)}{\zeta-\omega}. \tag{2.19}$$

Assume that $a^{\rm lhs}(\omega,k^2)$ varies only slowly over the resonance region where $\sin\delta\neq 0$,[11] and write

$$a^{\rm lhs}(\omega,k^2)=a^{\rm lhs}(\omega_R,k^2)+[a^{\rm lhs}(\omega,k^2)-a^{\rm lhs}(\omega_R,k^2)]. \tag{2.20}$$

The second term will then only contribute to the nonresonant background. The resonant part of the amplitude can therefore be written as

$$a(\omega,k^2)\cong a^{\rm lhs}(\omega_R,k^2)\left[e^{i\delta(\omega)}\cos\delta(\omega)+e^{i\delta(\omega)}e^{\rho(\omega)}\frac{\mathcal{P}}{\pi}\int_1^\infty\frac{\sin\delta(\xi)e^{-\rho(\xi)}d\xi}{\xi-\omega}\right] \tag{2.21}$$

$$a(\omega,k^2)\equiv a^{\rm lhs}(\omega_R,k^2)\chi(\omega)\quad\text{(resonant part)}. \tag{2.22}$$

It is convenient to define a new function $\psi(\omega)$ by

$$\chi(\omega)=\exp\left[\frac{1}{\pi}\int_1^\infty dy\frac{\delta(y)}{y-\omega-i\epsilon}\right]\psi(\omega), \tag{2.23}$$

where

$$\psi(\omega)=\exp\left(-\frac{1}{\pi}\int_1^\infty dy\frac{\delta(y)}{y-\omega-i\epsilon}\right)+\frac{1}{\pi}\int_1^\infty\frac{\sin\delta(\xi)}{\xi-\omega-i\epsilon}\times\exp\left[-\frac{\mathcal{P}}{\pi}\int_1^\infty\frac{\delta(z)dz}{z-\xi}\right]d\xi. \tag{2.24}$$

$\psi(\omega)$ then has the following properties: (i) $\psi(\omega)$ is

[10] R. Omnès, Nuovo Cimento 8, 316 (1958).

[11] Note that in general there will be a contribution to the integral from the region where δ comes back down through $\frac{1}{2}\pi$.

analytic in ω with a cut from $\omega=1$ to $\omega=\infty$; (ii) $\psi(\omega)\to 1$ as $\omega\to\infty$. Therefore, an unsubtracted dispersion relation can be written for the quantity $\psi(\omega)-1$:

$$\psi(\omega)-1=\frac{1}{\pi}\int_1^\infty d\omega'\frac{\mathrm{disc}\psi(\omega')}{\omega'-\omega}. \tag{2.25}$$

But from the above

$$\mathrm{disc}\psi(\omega)=\sin\delta(\omega)$$

$$\times\exp\left(-\frac{1}{\pi}\mathcal{P}\int_1^\infty dy\frac{\delta(y)}{y-\omega}\right)[-1+1]\equiv 0. \tag{2.26}$$

This leads to the conclusions that

$$\psi(\omega)=1, \tag{2.27}$$

$$a(\omega,k^2)=a^{\mathrm{lhs}}(\omega_R,k^2)/D(\omega), \tag{2.28}$$

$$D(\omega)=\exp\left(-\frac{1}{\pi}\int_1^\infty d\omega'\frac{\delta(\omega')}{\omega'-\omega-i\epsilon}\right), \tag{2.29}$$

which is the previous model result for the resonant multipole amplitude together with an explicit expression for $D(\omega)$, relating it entirely to the strong-interaction phase shift $\delta(\omega)$. One can now try to extend the present approach into the inelastic region.[12] This is discussed in Sec. 3.

3. TWO-CHANNEL MODEL

It is important for the inelastic resonances to extend the previous discussion of the Omnès equation to the coupled-channel case. Suppose that only two channels of the coupled-channel problem are important.[13] Let the two channels be denoted by $|1\rangle$ (the elastic channel) and $|2\rangle$. The strong-interaction S matrix for a given J^π then takes the form

$$S=\begin{pmatrix}S_{11} & S_{12}\\ S_{12} & S_{22}\end{pmatrix}. \tag{3.1}$$

This matrix is symmetric by time reversal and satisfies the unitarity condition

$$S^\dagger S=1. \tag{3.2}$$

Such a matrix can always be diagonalized with a real rotation. Defining new eigenstates by

$$|e_i\rangle=\sum_{j=1}^{2}R_{ij}|j\rangle, \tag{3.3}$$

where

$$R=\begin{pmatrix}\cos\varepsilon & \sin\varepsilon\\ -\sin\varepsilon & \cos\varepsilon\end{pmatrix}, \tag{3.4}$$

the S matrix takes the form

$$S_e=RSR^{-1}. \tag{3.5}$$

ε can now be chosen so that S_e is diagonal and therefore of the form

$$S_e=\begin{pmatrix}e^{2i\xi_1} & 0\\ 0 & e^{2i\xi_2}\end{pmatrix}. \tag{3.6}$$

Writing

$$S=R^{-1}S_eR, \tag{3.7}$$

a general representation of the two-channel S matrix is obtained in terms of three real quantities: two eigenphase shifts and a mixing angle. Defining a transition matrix by

$$S=1+2iT, \tag{3.8}$$

this general representation can be written as

$$T=\begin{pmatrix}e^{i\xi_1}\sin\xi_1\cos^2\varepsilon+e^{i\xi_2}\sin\xi_2\sin^2\varepsilon & \frac{1}{2}\sin 2\varepsilon(e^{i\xi_1}\sin\xi_1-e^{i\xi_2}\sin\xi_2)\\ \frac{1}{2}\sin 2\varepsilon(e^{i\xi_1}\sin\xi_1-e^{i\xi_2}\sin\xi_2) & e^{i\xi_1}\sin\xi_1\sin^2\varepsilon+e^{i\xi_2}\sin\xi_2\cos^2\varepsilon\end{pmatrix}. \tag{3.9}$$

The simplest model of an inelastic resonance is to say that one of the eigenphase shifts is resonant[14]:

$$e^{i\xi_1}\sin\xi_1=-\tfrac{1}{2}\Gamma/(W-W_R+\tfrac{1}{2}i\Gamma), \tag{3.10}$$

while the sine of the other eigenphase shift is small,

$$\xi_2\cong n\pi. \tag{3.11}$$

In that case the strong-interaction T matrix takes the form

$$T=e^{i\xi_1}\sin\xi_1\begin{pmatrix}\cos^2\varepsilon & \sin\varepsilon\cos\varepsilon\\ \sin\varepsilon\cos\varepsilon & \sin^2\varepsilon\end{pmatrix}. \tag{3.12}$$

The elastic amplitude is therefore parametrized by

$$(e^{2i\delta_1}-1)/2i=(\cos^2\varepsilon)e^{i\xi_1}\sin\xi_1, \tag{3.13}$$

and this equation can be used to determine both ε and ξ_1 for a given complex δ_1. Since the reaction cross section is determined by

$$|S_{12}|^2=1-|S_{11}|^2, \tag{3.14}$$

it will also be given correctly by this same parametrization. In the sharp-resonance case,

$$|T_{11}|^2=\tfrac{1}{4}\Gamma_1^2/[(W-W_R)^2+\tfrac{1}{4}\Gamma^2], \tag{3.15}$$

$$|T_{12}|^2=\tfrac{1}{4}\Gamma_1\Gamma_2/[(W-W_R)^2+\tfrac{1}{4}\Gamma^2], \tag{3.16}$$

where

$$\Gamma_1/\Gamma=\cos^2\varepsilon, \tag{3.17}$$

$$\Gamma_2/\Gamma=\sin^2\varepsilon. \tag{3.18}$$

[12] Note that it is not at all obvious what one should do with Eq. (2.29) when δ becomes complex.

[13] The results of this section can easily be extended to any number of channels.

[14] Y. Yamaguchi, Progr. Theoret. Phys. (Kyoto) Suppl. 7, 1 (1959).

These are just the two-channel Breit-Wigner formulas.

Suppose now that one includes the electroproduction channels

$$\gamma^*+N \nearrow |1\rangle \quad \searrow |2\rangle. \tag{3.19}$$

The complete S matrix then takes the form (to order e)[15]

$$S=\begin{pmatrix} S_{11} & S_{12} & 2ia_1 \\ S_{12} & S_{22} & 2ia_2 \\ 2ia_1 & 2ia_2 & 1 \end{pmatrix}. \tag{3.20}$$

The unitarity statement,

$$S^\dagger S=1, \tag{3.21}$$

now yields, in addition to the previously discussed strongly-coupled-channel conditions, the result (to order e)

$$\begin{pmatrix} \mathrm{Im}a_1 \\ \mathrm{Im}a_2 \end{pmatrix}=\begin{pmatrix} T_{11}^* & T_{12}^* \\ T_{21}^* & T_{22}^* \end{pmatrix}\begin{pmatrix} a_1 \\ a_2 \end{pmatrix}. \tag{3.22}$$

Notice that these relations are linear in the a's. In the approximation that only one eigenphase shift is resonant these equations become

$$\begin{pmatrix} \mathrm{Im}a_1 \\ \mathrm{Im}a_2 \end{pmatrix}=e^{-i\xi}\sin\xi\begin{pmatrix} \cos^2\varepsilon & \sin\varepsilon\cos\varepsilon \\ \sin\varepsilon\cos\varepsilon & \sin^2\varepsilon \end{pmatrix}\begin{pmatrix} a_1 \\ a_2 \end{pmatrix}. \tag{3.23}$$

Using this unitarity condition, the coupled Omnès equations for the electroproduction amplitudes can be written in the form[16]

$$a_1(\omega,k^2)=a_1^{\mathrm{lhs}}(\omega,k^2)+\frac{1}{\pi}\int_1^{\omega_t}\frac{e^{-i\xi}\sin\xi a_1(\omega',k^2)d\omega'}{\omega'-\omega-i\epsilon} +\frac{1}{\pi}\int_{\omega_t}^{\infty}\frac{e^{-i\xi}\sin\xi A_1(\omega',k^2)\cos\varepsilon d\omega'}{\omega'-\omega-i\epsilon}, \tag{3.24}$$

$$a_2(\omega,k^2)=a_2^{\mathrm{lhs}}(\omega,k^2)+\frac{1}{\pi}\int_1^{\omega_t}\frac{T_{21}^* a_1(\omega',k^2)d\omega'}{\omega'-\omega-i\epsilon} +\frac{1}{\pi}\int_{\omega_t}^{\infty}\frac{e^{-i\xi}\sin\xi A_1(\omega',k^2)\sin\varepsilon d\omega'}{\omega'-\omega-i\epsilon}. \tag{3.25}$$

In these expressions, the physical threshold for channel $|2\rangle$ has been denoted by ω_t, and

$$A_1(\omega,k^2)=\cos\varepsilon\ a_1(\omega,k^2)+\sin\varepsilon\ a_2(\omega,k^2). \tag{3.26}$$

Recalling that the linear combination of states which is assumed to resonate is

$$|e_1\rangle=\cos\varepsilon\,|1\rangle+\sin\varepsilon\,|2\rangle, \tag{3.27}$$

one observes that $A_1(\omega,k^2)$ is just the amplitude to produce this resonant channel.

[15] Only one electroproduction multipole is considered for clarity, but the results are easily seen to hold for all of them.

[16] Note that use has been made of the continuation of the unitarity relation below threshold in Eq. (3.25).

As a preliminary step in getting an approximate solution to these coupled Omnès equations, note that the analytic properties of the strong-interaction T-matrix elements of Eq. (3.9) are well known, and they have both right-hand and left-hand singularities. It will be assumed that $\sin\varepsilon(\omega)$ and $\cos\varepsilon(\omega)$, which are real along the right-hand cut and presumably slowly varying there, have only left-hand singularities. It is clear, at least in the model of Eq. (3.12), that one can do this since the amplitudes $T/e^{i\xi}\sin\xi$ then no longer have absorptive parts along the right-hand physical unitarity cut.

Suppose now that the following conditions hold: (i) There is a resonance in the first eigenchannel at an energy well above ω_t. (ii) In this region $a_{1,2}^{\mathrm{lhs}}(\omega,k^2)$, $\cos\varepsilon(\omega)$, and $\sin\varepsilon(\omega)$, which have only left-hand singularities, are slowly varying functions of ω. (iii) $A_{1,2}^{\mathrm{lhs}}(\omega,k^2)$ correctly describe the excitation functions, or the contributions from the left-hand regions, in the two eigenchannels. Note that this condition always lies at the heart of this approach, since one is forced to make some model of the contribution of the left-hand region.

Then by assumption (i), the first integral in Eq. (3.24) will be neglected in examining $a_1(\omega,k^2)$ in the resonance region. The first integral in Eq. (3.25) will be similarly neglected although the justification here is not so obvious since one must know $T_{21}^*(\omega)$ in this region, and this depends on a further model of the strong-interaction dynamics. It is assumed that this unphysical region does not play an important role in the resonance dynamics.[17] A linear combination of Eqs. (3.24) and (3.25) then yields

$$A_1(\omega,k^2) =A_1^{\mathrm{lhs}}(\omega,k^2)+\frac{1}{\pi}\int_{\omega_t}^{\infty}\frac{e^{-i\xi(\omega')}\sin\xi(\omega')A_1(\omega',k^2)d\omega'}{\omega'-\omega-i\epsilon} \times[\cos\varepsilon(\omega')\cos\varepsilon(\omega)+\sin\varepsilon(\omega')\sin\varepsilon(\omega)] \tag{3.28}$$

$$A_1(\omega,k^2)\equiv A_1^{\mathrm{lhs}}(\omega_1,k^2)+\Delta A_1(\omega,k^2). \tag{3.29}$$

By assumption (ii), $\Delta A_1(\omega,k^2)$ is an analytic function of ω with both a right-hand unitarity cut and left-hand singularities coming from $\sin\varepsilon(\omega)$ and $\cos\varepsilon(\omega)$. It therefore satisfies a dispersion relation

$$\Delta A_1(\omega,k^2)=\frac{1}{\pi}\int_{\mathrm{lhs}}\frac{\mathrm{disc}\Delta A_1(\omega',k^2)d\omega'}{\omega'-\omega-i\epsilon} +\frac{1}{\pi}\int_{\mathrm{rhs}}\frac{\mathrm{disc}\Delta A_1(\omega',k^2)d\omega'}{\omega'-\omega-i\epsilon}. \tag{3.30}$$

The first integral represents a rescattering correction to the excitation function and by assumption (iii), it

[17] We are aware of the fact that some authors would dispute this. This approximation is under further investigation using some simple models.

will be neglected. To evaluate the second integral, observe that on the right-hand cut

$$\text{disc}[(\omega'-\omega-i\epsilon)^{-1}(\cos\varepsilon(\omega)\cos\varepsilon(\omega') + \sin\varepsilon(\omega)\sin\varepsilon(\omega'))]=\pi\delta(\omega-\omega'). \quad (3.31)$$

The amplitude A_1 of Eq. (3.29) can therefore be written as

$$A_1(\omega,k^2)=A_1{}^{\text{lhs}}(\omega,k^2) + \frac{1}{\pi}\int_{\omega_t}^{\infty}\frac{e^{-i\xi}\sin\xi A_1(\omega',k^2)d\omega'}{\omega'-\omega-i\epsilon}. \quad (3.32)$$

[Note that this result follows immediately if ε is assumed to be a slowly varying function of ω in Eq. (3.28).] Using assumption (i) again, the integral can be extended down to $\omega=1$, using the elastic phase shift which is continuous with ξ at $\omega=\omega_t$. Thus, one can finally write

$$A_1(\omega,k^2)=A_1{}^{\text{lhs}}(\omega,k^2) + \frac{1}{\pi}\int_{1}^{\infty}\frac{e^{-i\xi}\sin\xi A_1(\omega',k^2)d\omega'}{\omega'-\omega-i\epsilon}. \quad (3.33)$$

This is just the equation which was discussed in the previous section, however, and with the stated approximations the resonant part of this eigenamplitude can therefore be written (returning now to the variables W and k^2)

$$A_1(W,k^2)=A_1{}^{\text{lhs}}(W,k^2)/D(W), \quad (3.34)$$

where $D(W)$ is now given in terms of the real eigenphase shift by

$$D(W)=\exp\left[-\frac{1}{\pi}\int_{W_0}^{\infty}dW'\frac{\xi(W')}{W'-W-i\epsilon}\right]. \quad (3.35)$$

Equation (3.34) can be rewritten

$$A_1(W,k^2)=[a_1{}^{\text{lhs}}(W,k^2)\cos\varepsilon + a_2{}^{\text{lhs}}(W,k^2)\sin\varepsilon]/D(W). \quad (3.36)$$

Note that

$$\cos^2\varepsilon=\Gamma_1/\Gamma, \quad (3.37)$$

$$\sin^2\varepsilon=\Gamma_2/\Gamma, \quad (3.38)$$

so the magnitude of ε is directly related to physical quantities. There is, however, no way to determine the *sign* of ε from the development presented here, so this quantity is still a parameter for each resonance. In all our derivations, the integrals have been assumed to be convergent as written; this final model result, however, will be considered to have more general validity.

An exactly analogous discussion of $A_2(W,k^2)$ shows that the discontinuity on the right-hand cut vanishes, and therefore $A_2(W,k^2)$ will be nonresonant. By inverting Eq. (3.3), the resonant contributions to the amplitudes $a_{1,2}(W,k^2)$ can therefore be written as

$$a_1(W,k^2)=A_1(W,k^2)\cos\varepsilon, \quad (3.39)$$

$$a_2(W,k^2)=A_1(W,k^2)\sin\varepsilon. \quad (3.40)$$

In inelastic electron scattering experiments where only the electrons are detected one evidently measures the quantity

$$\int_{\text{Res}}dW|a_1(W,k^2)|^2+\int_{\text{Res}}dW|a_2(W,k^2)|^2 = \int_{\text{Res}}dW|A_1(W,k^2)|^2. \quad (3.41)$$

The resonance in the eigenchannel can again be defined by

$$\text{Re}D(W_R)=0, \quad (3.42)$$

and just as before

$$\int_{\text{Res}}dW|A_1(W,k^2)|^2=\frac{2\pi}{\Gamma}|[a_1{}^{\text{lhs}}(W_R,k^2)\cos\varepsilon + a_2{}^{\text{lhs}}(W_R,k^2)\sin\varepsilon]/\text{Re}'D(W_R)|^2. \quad (3.43)$$

Several limiting cases of this result are of interest [the positive square root is taken in Eqs. (3.37) and (3.38) for definiteness].

(i) If $a_1{}^{\text{lhs}}(W_R,k^2)\cong a_2{}^{\text{lhs}}(W_R,k^2)$ and

(a) $\Gamma_1\cong\Gamma_2$, then

$$\int_{\text{Res}}dW|A_1(W,k^2)|^2=\frac{2\pi}{\Gamma}\frac{\Gamma}{\Gamma_1}\left|\frac{a_1{}^{\text{lhs}}(W_R,k^2)}{\text{Re}'D(W_R)}\right|^2; \quad (3.44)$$

(b) $\Gamma_2\ll\Gamma_1$, then

$$\int_{\text{Res}}dW|A_1(W,k^2)|^2=\frac{2\pi}{\Gamma}\left|\frac{a_1{}^{\text{lhs}}(W_R,k^2)}{\text{Re}'D(W_R)}\right|^2. \quad (3.45)$$

Both of these results are just the *previous results of model I, only now with an explicit prescription for computing $D(W)$ when inelastic channels are present.*

(ii) If $a_1{}^{\text{lhs}}(W_R,k^2)\gg a_2{}^{\text{lhs}}(W_R,k^2)$, then

$$\int_{\text{Res}}dW|A_1(W,k^2)|^2=\frac{2\pi}{\Gamma}\frac{\Gamma_1}{\Gamma}\left|\frac{a_1{}^{\text{lhs}}(W_R,k^2)}{\text{Re}'D(W_R)}\right|^2, \quad (3.46)$$

and the result is smaller than that of model I if $\Gamma_1<\Gamma$ since the resonance is not as strongly formed in this case.

This model explicitly keeps only two channels which are assumed to be the important channels in the resonance regions. As $W\to\infty$, many more channels will open, and it is reasonable to assume that the amplitudes become purely absorptive, or purely imaginary, in this limit. Thus it might be expected that

$$\xi\xrightarrow[W\to\infty]{}\tfrac{1}{2}\pi. \quad (3.47)$$

There is experimental evidence (see Sec. 4) that this is indeed happening. In this case, one must make a subtraction in the expression for D and write

$$D(W)=\exp\left[-\frac{(W-M_s)}{\pi}\times\int_{W_0}^{\infty}\frac{dW'\xi(W')}{(W'-M_s)(W'-W-i\epsilon)}\right], \quad (3.48)$$

$$D(M_s)=1. \quad (3.49)$$

The absolute normalization of the resonance amplitude is therefore expressed in terms of the subtraction point M_s.[18]

4. CALCULATION OF $D(W)$

This section is devoted to the determination of the eigenphase shift ξ for the various resonances and the calculation of $D(W)$ as an integral over ξ as given by Eq. (3.48). With the assumption of only one nonzero eigenphase, the elastic amplitude in a particular channel has the parametrization of Eq. (3.13):

$$(e^{2i\delta_1}-1)/2i=(\cos^2\varepsilon)e^{i\xi}\sin\xi. \quad (4.1)$$

δ_1 is the (complex) π-N phase shift for the given channel:

$$\delta_1=\delta_R+i\delta_I. \quad (4.2)$$

Extensive phase-shift analyses of pion-nucleon scattering have been performed by several groups[19–21] with the result that there is substantial agreement on the phases δ_1 up to c.m. energies of the order of 2 GeV.[22]

As discussed in Ref. 8, it is only the resonant phase shift that is of interest here. Thus, one needs to decompose δ_1 into a resonant part and a background part. In many channels, however, there appears to be no appreciable background, and so δ_1 is the resonant phase. Such is the case for the P_{33}, D_{13}, D_{15}, F_{15}, and F_{37} channels,[23] and these are the channels that will be considered here. The S_{31} channel is an example where there is a significant nonresonant contribution to the phase shift. In the S_{11} channel there are two low-lying resonances that overlap each other considerably.[19,21,22] Consequently, the assumption of a single resonant eigenchannel is no longer adequate, and a more sophisticated treatment of the S_{11} channel is required.

Equation (4.1) determines both ξ and the magnitude of ε:

$$\tan\xi=(1-\eta\cos2\delta_R)/\eta\sin2\delta_R, \quad (4.3)$$

$$\cos^2\varepsilon\equiv\Gamma_1/\Gamma=1-\tfrac{1}{2}(1-\eta^2)/(1-\eta\cos2\delta_R), \quad (4.4)$$

where

$$\eta\equiv\exp(-2\delta_I). \quad (4.5)$$

The phase-shift analyses give values of δ_R and η. In calculating ξ and Γ_1/Γ the CERN dispersion relation fits to δ_R and η have been used,[20] and eigenphase shifts and ratios of Γ_1/Γ have been evaluated for the P_{33}, D_{13}, D_{15}, F_{15}, and F_{37} channels. The following features were noted:

(i) When $\eta=1$ (i.e., $\delta_I=0$), then $\xi\equiv\delta_1$ and $\Gamma_1/\Gamma\equiv1$.

(ii) The behavior of δ_R near a resonance depends critically on the value of Γ_1/Γ. If $\Gamma_1/\Gamma>0.5$, then δ_R rises through $\frac{1}{2}\pi$ at resonance. This, happens, for example, in the P_{33}, D_{13}, and F_{15} channels. But if $\Gamma_1/\Gamma<0.5$, then δ_R falls sharply through zero at resonance and becomes negative. Examples are found in the D_{15} and F_{37} channels. The eigenphase shift, however, shows no such dependence on Γ_1/Γ. In all the cases under consideration ξ rises through $\frac{1}{2}\pi$ at resonance. Thus $D(W)$ as defined in Eq. (3.35) will be pure imaginary at resonance, and this justifies the definition (3.42).

(iii) Goldberg[24] has observed that small changes in the eigenphase shift and mixing angle can produce rapid changes in the phase shift δ_R and inelasticity η. The results of the present calculation substantiate this observation. One example is the contrast noted above between the behavior of ξ and δ_R for Γ_1/Γ just greater than and just less than 0.5. Even in the cases where δ_R goes through $\frac{1}{2}\pi$ at resonance, the slope of the eigenphase shift is less steep than that of δ_R. This is particularly apparent in the D_{13} channel where δ_R rises almost vertically through $\frac{1}{2}\pi$. The increase of ξ is much less rapid.

(iv) Γ_1/Γ is reasonably constant over the region of the resonance. This justifies the assumption that $\varepsilon(W)$ is a slowly varying function over the resonance. (See Sec. 3.)

(v) The CERN analysis extends to $W=2.189$ GeV. Before this energy is reached, the eigenphase shifts have all come back down close to or through $\frac{1}{2}\pi$, and all but that in the F_{37} channel have reached a minimum and started rising again. Thus, unlike δ_R, the eigenphase shift does not appear to approach either π or 0 asymptotically. Indeed, it appears to be oscillat-

[18] In the discussions of this section it is assumed that the multipole amplitudes have been so chosen that Eqs. (3.22) and (3.41) hold. These equations do not depend on the normalization of the initial state γ^*+N but do depend on that of the strongly interacting particles. These normalizations can be chosen following Jacob and Wick (Ref. 32). In the notation of I it is the amplitudes $\langle\lambda_2|T^J(W,k^2)|\lambda_1\lambda_k\rangle$ which are being discussed.

[19] P. Bareyre, C. Bricman, and G. Villet, Phys. Rev. **165**, 1730 (1968).

[20] A. Donnachie, R. G. Kirsopp, and C. Lovelace, Phys. Letters **26B**, 161 (1968); CERN Report No. TH. 838, Addendum, 1967 (unpublished).

[21] C. Johnson and H. Steiner, Lawrence Radiation Laboratory Report No. UCRL-18001, 1967 (unpublished); C. Johnson, Lawrence Radiation Laboratory Report No. UCRL-17683, 1967 (unpublished).

[22] C. Lovelace, in *Proceedings of the Heidelberg International Conference on Elementary Particles, 1967* (North-Holland Publishing Co., Amsterdam, 1968), p. 79.

[23] The usual notation is used where the letter indicates the orbital angular momentum of the $|\pi N\rangle$ system and the subscripts are $2T$, $2J$, with T the isospin and J the total spin of the resonance.

[24] Hyman Goldberg, Phys. Rev. **151**, 1186 (1966).

ing about $\frac{1}{2}\pi$ as W increases. As noted earlier there are theoretical reasons for assuming that the amplitudes become pure imaginary as $W\to\infty$, and the behavior of the eigenphase shift tends to support this conclusion.

After the eigenphase shift has been obtained, $D(W)$ as given in Eq. (3.35) can be evaluated. In order to do this, the eigenphase shift $\xi(W)$ is needed for $m+\mu \leq W<\infty$. For $m+\mu\leq W\leq 2.189$ GeV, $\xi(W)$ has been determined from the phase-shift analysis. For $W>2.189$ GeV an additional assumption must be made. Following the argument in (v) above, it is assumed that $\xi(W)\equiv\frac{1}{2}\pi$ for $W>2.189$ GeV. With this assumption it is necessary to make a subtraction in the expression for $D(W)$ as indicated in Eqs. (3.48) and (3.49). The integral in Eq. (3.48) can be rewritten as

$$D(W)=\lim_{W_c\to\infty}[\bar{D}(W)/\bar{D}(M_s)], \tag{4.6}$$

where

$$\bar{D}(W)\equiv\exp\left(-\frac{1}{\pi}\int_{m+\mu}^{W_c}dW'\frac{\xi(W')}{W'-W-i\epsilon}\right). \tag{4.7}$$

The absolute normalization of $D(W)$ therefore depends on the subtraction point M_s, and M_s will only be determined later by comparison with experiment. However, the behavior of D as a function of W, that is the shape of the resonance, is independent of M_s.

The integral in Eq. (3.48) has been performed numerically, and in Fig. 2, $|1/D(W)|^2$ is plotted for the D_{13}, D_{15}, F_{15}, and F_{37} channels. The vertical scale was determined by taking M_s to be the proton mass. It is interesting to note that the maximum values are nearly the same for all four resonances. The predicted widths are considerably larger than the π-N widths listed in the Particle Data Group tables,[25] but they are only slightly larger than the widths found in the CERN phase-shift analysis.[20] These discrepancies are not so surprising when one recalls from atomic or nuclear physics that predictions of widths depend critically on the particular model employed. In the present case the model is that of a single nonzero eigenphase. In all cases the energy at which $|1/D(W)|^2$ is a maximum lies below that at which ξ passes through $\frac{1}{2}\pi$. This is a commonly observed phenomenon in resonance cross sections.[26] [*Note added in proof.* After completion of this work we learned that a discrepancy has been found[26a] between the elastic π^-p scattering data and the CERN dispersion relation fit to the phase shifts[20] for 1.4 GeV $\lesssim W\lesssim$ 1.8 GeV. The calculations of this section have been repeated using the Glasgow phase shifts,[26b] which do show qualitative agreement with the π^-p data.[26a] The widths of the higher resonances are considerably reduced and are now consistent with the tabulated π-N widths.[25] In addition, the maximum of $|1/D(W)|^2$ is now only 12–15 MeV below the energy at which ξ passes through $\frac{1}{2}\pi$ (rather than 50–60 MeV as was the case with the CERN results). Both of these changes lead to much better agreement with the results of the SLAC experiments (see Sec. 7)].

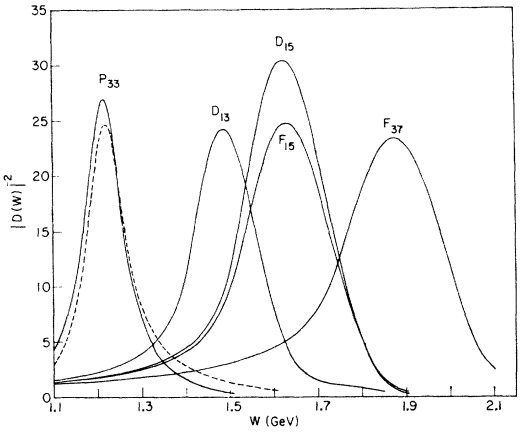

FIG. 2. $1/|D(W)|^2$ from Eqs. (3.47) and (3.48) for the P_{33}, D_{13}, D_{15}, F_{15}, and F_{37} channels. The vertical scale is determined by taking $M_s=m$. The dashed curve for the P_{33} channel shows $0.5/|D(W)|^2$ computed using δ_R above the inelastic threshold.

The 3-3 resonance occurs below the inelastic threshold, and Eq. (2.29), which gives $D(W)$ as an integral over the elastic phase shift, should be applicable to this resonance. Figure 2 shows the result for $|1/D(W)|^2$ calculated using δ_R above the inelastic threshold. It has been assumed that $\delta_R\equiv\pi$ for $W>2.189$ GeV, in accord with the present experimental indications and $M_s=m$. Unlike the higher resonances, the predicted width is slightly smaller than that found in π-N scattering; the location of the maximum, however, is again shifted below the resonance energy. It is interesting to note that if one evaluates $D(W)$ for the 3-3 resonance using the treatment of the inelastic region implied by Eq. (3.48) (again assuming $\xi\equiv\frac{1}{2}\pi$ for $W>2.189$ GeV), the resulting shape is almost identical to that given by the integral over the elastic phase shift. This is illustrated in Fig. 2. The normalization, however, is substantially different. $|1/D(W_R)|^2=27.0$ when the eigenphase shift is used compared with $|1/D(W_R)|^2=49.3$ from the elastic phase shift. This suggests that even for the 3-3 resonance the contribution of the inelastic region may be significant for the over-all normalization.

One should note that the approximation

$$A_1(W,k^2)\cong A_1^{\rm lhs}(W_R,k^2)/D(W) \tag{4.8}$$

[25] N. Barash-Schmidt, A. Barbaro-Galtieri, L. R. Price, Matts Roos, A. H. Rosenfeld, Paul Soding, and C. G. Wohl, Lawrence Radiation Laboratory Report No. UCRL-8030, 1968 (unpublished).

[26] Gunnar Källén, *Elementary Particle Physics* (Addison-Wesley Publishing Co., Inc., Reading, Mass., 1964), p. 145.

[26a] A. D. Brody, D. W. G. S. Leith, B. G. Levi, B. C. Shen, D. Herndon, R. Longacre, L. Price, A. H. Rosenfeld, and P. Soding, Phys. Rev. Letters **22**, 1401 (1969).

[26b] A. T. Davies and R. G. Moorhouse, in *Proceedings of the Fourteenth International Conference on High-Energy Physics, Vienna, 1968* (CERN, Geneva, 1968). We thank Professor Moorhouse for permission to use these results prior to publication.

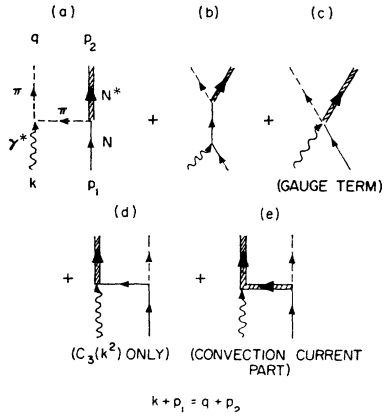

FIG. 3. Assumed excitation mechanism for electroproduction of $|\pi N^*(1236)\rangle$ channel.

used for all numerical calculations does not preserve the threshold behavior in W since the numerator on the right side is evaluated at W_R. Consequently, the shapes of the resonances presented in Fig. 2 are less reliable near threshold.

5. EXCITATION MECHANISM

A model for the excitation function $a^{\text{lhs}}(W,k^2)$ is now made by choosing a gauge-invariant set of exchange graphs which are assumed to play a dominant role in the excitation process. The graphs used for the $|\pi N\rangle$ channel were discussed and evaluated in I. The graphs used to evaluate the $|\pi N^*(1236)\rangle$ channel excitation function $a_2{}^{\text{lhs}}(W,k^2)$ are shown in Fig. 3. In this model the excitation graphs are treated as generalized Feynman amplitudes in the sense that renormalized coupling constants and measured form factors are used at each vertex. This amplitude thus correctly reproduces all the pole terms in any dispersion theory treatment of the process. Away from the poles this is just a simple model of the process which, however, maintains the general properties of the theory.

Since the excitation of the $N^*(1236)$ is known to be predominantly a magnetic dipole transition (at least for small k^2), the γNN^* vertex is approximated by[1,27]

$$ie[C_3(k^2)/m_\pi]\gamma_5[k_\nu\gamma_\mu-(\gamma\cdot k)\delta_{\mu\nu}], \tag{5.1}$$

where the index ν refers to the spinor $\bar{w}_\nu(p_2,\lambda_2)$ for the $J=\frac{3}{2}$ isobar, μ refers to the photon polarization $\epsilon_\mu(\lambda_k)$, and k is the incoming virtual photon's four-momentum. This vertex is gauge-invariant by itself since it vanishes when multiplied by k_μ. The form factor $C_3(k^2)$ is determined by computing the transverse cross section for electron excitation of the $N^*(1236)$ resonance using (5.1) and equating this with the experimental value (see Fig. 4)

$$[C_3(k^2)]^2 = \frac{4m_\pi{}^2M^4[|f_+|^2+|f_-|^2]_{\text{expt}}}{[(M-m)^2+k^2][M^2(M+m)^2+\frac{1}{3}(k^2+Mm+m^2)^2]}, \tag{5.2}$$

where M is the mass of the $N^*(1236)$. The πNN^* vertex is obtained from the phenomenological interaction

$$\mathcal{L}_I=\gamma_\pi\bar{\psi}_{\mu i}\psi\partial\phi_i/\partial x_\mu+\text{h.c.} \tag{5.3}$$

Using this interaction, the decay width for $p^*\to p+\pi^0$ is

$$\Gamma(p^*\to p+\pi^0) = \frac{\gamma_{\pi^0}{}^2[(M^2-m^2-m_\pi{}^2)^2-4m_\pi{}^2m^2]^{3/2}[(M+m)^2-m_\pi{}^2]}{12\pi(16M^5)}. \tag{5.4}$$

From the experimental value of 80 MeV, one obtains

$$(\gamma_{\pi^0})^2=(79.7\text{ MeV})^{-2}. \tag{5.5}$$

The coupling constants for the charged mesons needed in Fig. 3 follow from isotopic spin invariance:

$$\begin{aligned}\gamma_{\pi^+}&=-\tfrac{1}{2}\sqrt{2}\gamma_{\pi^0},\\ \gamma_{\pi^-}&=-\tfrac{1}{2}(\sqrt{6})\gamma_{\pi^0}=-\gamma_\pi.\end{aligned} \tag{5.6}$$

Similarly,

$$C_3(k^2)_{p^*p}=C_3(k^2)_{n^*n}. \tag{5.7}$$

By comparing the amplitude for pion electroproduction computed using an N and $N^*(1236)$ in the direct channel with the results of CGLN,[28] one finds that

$$eC_3(0)\gamma_{\pi^0}/eg_{\pi^0N}>0. \tag{5.8}$$

Equations (5.6) to (5.8) suffice to determine all the necessary relative signs in Fig. 3. Our phase convention will be to take both γ_{π^0} and $C_3(0)$ as positive. Since the interaction in Eq. (5.3) is a derivative coupling, graph (c) must be included whenever a charged pion is emitted. It is included with a form factor $F_G(k^2)$. Only the terms from the N^* exchange graph (e) which include the convection current and are necessary for gauge invariance are kept.[29] Since the $N^*(1236)$ has isospin $\frac{3}{2}$, conservation of isospin here rules out the ω^0 exchange graph, which was found to be important in I. The resulting generalized Feynman amplitude for electroproduction of the $|\pi N^*(1236)\rangle$ channel from a proton target can finally be expressed as

$$[2\omega_qE_1E_2\Omega^3/mM]^{1/2}\langle qp_2{}^{(-)}|J_\mu(0)|p_1\rangle\epsilon_\mu = -\bar{w}_\nu(p_2)A_{\nu\mu}\epsilon_\mu u(p_1), \tag{5.9}$$

[27] M. Gourdin and Ph. Salin, Nuovo Cimento **27**, 193 (1963); **27**, 309 (1963).

[28] G. F. Chew, M. L. Goldberger, F. E. Low, and Y. Nambu, Phys. Rev. **106**, 1337 (1957); **106**, 1345 (1957); referred to hereafter as CGLN.

[29] The numerator in the N^* propagator is replaced by the approximate form $\delta_{\nu\lambda}-\frac{1}{3}\gamma_\nu\gamma_\lambda$ and $F_1{}^{N^*}(k^2)\gamma_\mu$ is used for the electromagnetic vertex [see Eqs. (5.10) and (5.12)].

$$A_{\nu\mu}{}^{+}=\sqrt{2}g_{\pi N}[C_3/m_\pi]\gamma_5[k_\nu\gamma_\mu-(\gamma\cdot k)\delta_{\mu\nu}]$$
$$\times[i(\gamma\cdot p_2-\gamma\cdot k)+m]^{-1}\gamma_5-i\gamma_\pi{}^{+}\{F_G\delta_{\mu\nu}-(q-k)_\nu$$
$$\times(2q-k)_\mu F_\pi[(q-k)^2+m_\pi{}^2]^{-1}-iq_\nu$$
$$\times[i(\gamma\cdot p_1+\gamma\cdot k)+m]^{-1}(F_1{}^p\gamma_\mu-F_2{}^p\sigma_{\mu\lambda}k_\lambda)$$
$$-i\gamma_\mu F_1{}^{n^*}[i(\gamma\cdot p_2-\gamma\cdot k)+M]^{-1}$$
$$\times[q_\nu-\tfrac{1}{3}\gamma_\nu(\gamma\cdot q)]\},\quad(5.10)$$

$$A_{\nu\mu}{}^{0}=-g_{\pi N}(C_3/m_\pi)\gamma_5[k_\nu\gamma_\mu-(\gamma\cdot k)\delta_{\mu\nu}]$$
$$\times[i(\gamma\cdot p_2-\gamma\cdot k)+m]^{-1}\gamma_5-i\gamma_{\pi^0}$$
$$\times\{-iq_\nu[i(\gamma\cdot p_1+\gamma\cdot k)+m]^{-1}(F_1{}^p\gamma_\mu-F_2{}^p\sigma_{\mu\lambda}k_\lambda)$$
$$-i\gamma_\mu F_1{}^{p^*}[i(\gamma\cdot p_2-\gamma\cdot k)+M]^{-1}$$
$$\times[q_\nu-\tfrac{1}{3}\gamma_\nu(\gamma\cdot q)]\},\quad(5.11)$$

$$A_{\nu\mu}{}^{-}=-i\gamma_\pi{}^{-}\{-F_G\delta_{\mu\nu}+(q-k)_\nu(2q-k)_\mu F_\pi$$
$$\times[(q-k)^2+m_\pi{}^2]^{-1}-iq_\nu[i(\gamma\cdot p_1+\gamma\cdot k)+m]^{-1}$$
$$\times(F_1{}^p\gamma_\mu-F_2{}^p\sigma_{\mu\lambda}k_\lambda)-i\gamma_\mu 2F_1{}^{N^{*++}}$$
$$\times[i(\gamma\cdot p_2-\gamma\cdot k)+M]^{-1}$$
$$\times[q_\nu-\tfrac{1}{3}\gamma_\nu(\gamma\cdot q)]\}.\quad(5.12)$$

In these expressions, the superscript on A refers to the charge of the emerging pion. Also $g_{\pi N}=g_{\pi^0 N}$ and $C_3=C_3{}^p=C_3{}^n$. All of the form factors are functions of k^2, as is C_3.

It immediately follows from these results that

$$A_{\nu\mu}{}^{+}k_\mu=-i\gamma_\pi{}^{+}[(F_G-F_\pi)k_\nu$$
$$+(F_\pi-F_1{}^p+F_1{}^{n^*})q_\nu],\quad(5.13)$$

$$A_{\nu\mu}{}^{0}k_\mu=-i\gamma_{\pi^0}[(F_1{}^{p^*}-F_1{}^p)q_\nu],\quad(5.14)$$

$$A_{\nu\mu}{}^{-}k_\mu=-i\gamma_\pi{}^{-}[(F_\pi-F_G)k_\nu$$
$$+(2F_1{}^{N^{*++}}-F_\pi-F_1{}^p)q_\nu].\quad(5.15)$$

This set of generalized Feynman amplitudes is therefore manifestly gauge-invariant if

$$F_G=F_\pi,\qquad F_1{}^{p^*}=F_1{}^p,$$
$$F_1{}^{N^{*++}}=\tfrac{1}{2}(F_\pi+F_1{}^p),\quad F_1{}^{n^*}=F_1{}^p-F_\pi.\quad(5.16)$$

Note that this is not a necessary condition for gauge invariance, but merely a sufficient one. One can always add terms proportional to k_μ to the amplitude without changing any of the physics of electroproduction since

$$k_\mu\epsilon_\mu=0\quad(5.17)$$

because of conservation of the electron current. Thus, for example, one could leave the physical amplitude unchanged by replacing

$$(2q-k)_\mu F_\pi\rightarrow(2q-k)_\mu F_\pi$$
$$+(F_1{}^V-F_\pi)(2q\cdot k-k^2)k_\mu/k^2\quad(5.18)$$

and obtain a manifestly gauge-invariant amplitude without requiring $F_\pi=F_1{}^V$, as was done in I.[30] The philosophy of the present model, however, is to do the simplest thing possible to obtain a manifestly gauge-invariant expression, and Eqs. (5.16) shall be assumed to hold. The elastic form-factor fits used in I will also be used here [see Eq. (6.2)]. In particular this means that $F_1{}^p=F_\pi$ so that $F_1{}^{n^*}=0$. The effect of possible alternative fits to the elastic form factors will be discussed in Sec. 6.

The amplitudes for production of a $|\pi N^*(1236)\rangle$ state of definite total isotopic spin from a proton target are related to the charged amplitudes by [only $T=\frac{1}{2},\frac{3}{2}$ are nonzero]

$$(\sqrt{15})A^{3/2}=(\sqrt{8})A^{+}-A^{0}-(\sqrt{6})A^{-},$$
$$(\sqrt{6})A^{1/2}=A^{+}-\sqrt{2}A^{0}+\sqrt{3}A^{-}.\quad(5.19)$$

It is easily demonstrated that the general amplitude for electroproduction of the $|\pi N^*(1236)\rangle$ channel involves 12 linearly independent gauge-invariant kinematic invariants. These can be taken to be $\gamma_5 q_\nu M_i$ and $\gamma_5 k_\nu M_i$, where M_i $(i=1\cdots6)$ are the invariants used in I. In fact, there are only nine combinations of invariants which naturally appear in the present calculation and these are[31]

$$(2\omega_q E_1E_2\Omega^3/mM)^{1/2}\langle qp_2{}^{(-)}|J_\mu(0)\epsilon_\mu|p_1\rangle$$
$$=\bar{w}_\nu(p_2\lambda_2)[\sum_{i=1}^{9}M_\nu{}^{(i)}A^{(i)}(W,k^2,k\cdot q)]u(p_1\lambda_1),$$
$$M_\nu{}^{A}=\tfrac{1}{2}iq_\nu[(\gamma\cdot\epsilon)(\gamma\cdot k)-(\gamma\cdot k)(\gamma\cdot\epsilon)],$$
$$M_\nu{}^{B}=2iq_\nu[(P\cdot\epsilon)(q\cdot k)-(P\cdot k)(q\cdot\epsilon)],$$
$$M_\nu{}^{C}=q_\nu[(\gamma\cdot\epsilon)(q\cdot k)-(\gamma\cdot k)(q\cdot\epsilon)],$$
$$M_\nu{}^{D}=2q_\nu[(\gamma\cdot\epsilon)(P\cdot k)-(\gamma\cdot k)(P\cdot\epsilon)]$$
$$-imq_\nu[(\gamma\cdot\epsilon)(\gamma\cdot k)-(\gamma\cdot k)(\gamma\cdot\epsilon)],\quad(5.20)$$
$$M_\nu{}^{E}=iq_\nu[(k\cdot\epsilon)(q\cdot k)-(q\cdot\epsilon)k^2],$$
$$M_\nu{}^{F}=i[\epsilon_\nu(q\cdot k)-k_\nu(q\cdot\epsilon)],$$
$$M_\nu{}^{G}=2i[\epsilon_\nu(P\cdot k)-k_\nu(P\cdot\epsilon)]$$
$$+(m+M)[\epsilon_\nu(\gamma\cdot k)-k_\nu(\gamma\cdot\epsilon)],$$
$$M_\nu{}^{H}=i[k_\nu(k\cdot\epsilon)-\epsilon_\nu k^2],$$
$$M_\nu{}^{I}=\tfrac{1}{2}ik_\nu[(\gamma\cdot\epsilon)(\gamma\cdot k)-(\gamma\cdot k)(\gamma\cdot\epsilon)].$$

In these expressions

$$P=\tfrac{1}{2}(p_1+p_2).\quad(5.21)$$

The coefficients $A^{(i)}(W,k^2,k\cdot q)$ obtained from Eqs. (5.9) and (5.20) are listed in Appendix A for each charge state of the pion. Because explicitly gauge-invariant M_ν's were chosen, the B and E coefficients contain an apparent $1/k\cdot q$ kinematic singularity. When these nine generalized Feynman amplitudes

[30] See for example, N. Kroll, in *International Conference on High-Energy Physics, Vienna, 1968* (CERN, Geneva, 1968), p. 78.

[31] These nine invariants can be expanded in terms of the 12 linearly independent invariants mentioned in the text by expanding ϵ_μ in terms of a complete orthonormal basis of four vectors constructed from P_μ, k_μ, q_μ, and $\epsilon_{\mu\nu\rho\sigma}P_\nu k_\rho q_\sigma$ and then using $\epsilon_{\mu\nu\rho\sigma}=(\gamma_5/24)[\gamma_\mu,\gamma_\nu,\gamma_\rho,\gamma_\sigma]_{\text{antisym}}$, the Dirac equation, and the subsidiary conditions on $\bar{w}_\nu(p_2)$.

are combined to give the transition matrix elements, this singularity disappears as it must. For the $|\pi N\rangle$ channel the same behavior occurred and was discussed in I.

In order to perform a Jacob-Wick helicity analysis, the c.m. frame of the $|\pi N^*(1236)\rangle$ system is chosen and the helicity amplitudes $\langle\lambda_2|T^J(W,k^2)|\lambda_1\lambda_k\rangle$ are projected explicitly in this frame (λ_k is the incident photon helicity). The vector magnitudes are denoted by

$$\begin{aligned} k^* &= |\mathbf{k}| = |\mathbf{p}_1|\,, \\ q^* &= |\mathbf{q}| = |\mathbf{p}_2|\,, \end{aligned} \tag{5.22}$$

while k_0, ω_q, E_1, and E_2 refer to the energies. The angles ϕ and θ are defined exactly as in I (see I, Fig. 4)

$$\begin{aligned} \hat{p}_1 &= (0,0,1)\,, \\ \hat{p}_2 &= (\sin\theta\cos\phi, \sin\theta\sin\phi, \cos\theta)\,. \end{aligned} \tag{5.23}$$

The scattering amplitude for $\gamma^*+N\rightarrow N^*(1236)+\pi$, defined by

$$f_{\lambda_2;\lambda_1\lambda_k}(\theta,\phi)\equiv+\frac{(mM)^{1/2}}{4\pi W}\bar{w}_\nu(p_2\lambda_2) \times\Big[\sum_{i=1}^{9} M_\nu^{(i)}(\lambda_k)A^{(i)}(W,k^2,k\cdot q)\Big]u(p_1\lambda_1)\,, \tag{5.24}$$

is expanded according to Jacob and Wick[32] [compare I, Eq. (3.13)]

$$f_{\lambda_2;\lambda_1\lambda_k}(\theta,\phi)=\frac{1}{(4k^*q^*)^{1/2}}\sum_J(2J+1) \times\mathfrak{D}_{\lambda_1-\lambda_k-\lambda_2}{}^J(-\phi,-\theta,\phi)^*\langle\lambda_2|T^J(W,k^2)|\lambda_1\lambda_k\rangle. \tag{5.25}$$

The angular momentum notation follows Edmonds.[33] Using the orthogonality of the $d_{m'm}{}^J(-\theta)$, Eq. (5.25) is inverted to give

$$\frac{1}{(4k^*q^*)^{1/2}}\langle\lambda_2|T^J(W,k^2)|\lambda_1\lambda_k\rangle =\frac{1}{2}\int_{-1}^{1}d(\cos\theta)f_{\lambda_2;\lambda_1\lambda_k}(\theta,\phi) \times\mathfrak{D}_{\lambda_1-\lambda_k,\lambda_2}{}^J(-\phi,-\theta,\phi). \tag{5.26}$$

In order to evaluate this integral, either analytically or numerically, it is necessary to exhibit the angular dependence of $f(\theta,\phi)$. Although the dependence of $A^{(i)}(W,k^2,k\cdot q)$ on θ is apparent from looking at Appendix A, the angular dependence of $\bar{w}_\nu(p_2\lambda_2)\times M_\nu^{(i)}(\lambda_k)u(p_1,\lambda_1)$ is hidden in the Dirac matrix multiplication and in the four-vector dot products which result from it. [Clearly each of the kinematic invariants can be treated separately in evaluating (5.26).] The intricate procedure of expanding these products in the c.m. frame is discussed in Appendix B.

Because there are three independent photon helicity states, there are 24 matrix elements of the form $\langle\lambda_2|T^J(W,k^2)|\lambda_1\lambda_k\rangle$ which need to be calculated. As a result of parity conservation in this reaction, only 12 of these are independent. It is then convenient to form parity eigenstates [compare I, Eq. (3.15)]

$$\langle\lambda_2{}^\pm|\equiv\tfrac{1}{2}\sqrt{2}[\langle\lambda_2|\mp\langle-\lambda_2|], \quad(\lambda_2=\tfrac{3}{2},\tfrac{1}{2}); \tag{5.27}$$

$$\begin{aligned} |\tfrac{3}{2}{}^\pm\rangle &\equiv\tfrac{1}{2}\sqrt{2}[|\lambda_1=-\tfrac{1}{2},\lambda_k=1\rangle\mp|\tfrac{1}{2}-1\rangle], \\ |\tfrac{1}{2}{}^\pm\rangle &\equiv\tfrac{1}{2}\sqrt{2}[|\tfrac{1}{2}1\rangle\mp|-\tfrac{1}{2}-1\rangle], \\ |L^\pm\rangle &\equiv\tfrac{1}{2}\sqrt{2}[|\tfrac{1}{2}0\rangle\mp|-\tfrac{1}{2}0\rangle]. \end{aligned} \tag{5.28}$$

The parity of these states is $(-1)^{J\pm1/2}$. In each parity channel there are six amplitudes, three to the $|\lambda_2|=\frac{3}{2}$ final state and three to the $|\lambda_2|=\frac{1}{2}$ state. Thus, the $|\pi N^*(1236)\rangle$ excitation contributes to two independent final-state channels in the T matrix.

The approach of this calculation, however, is to consider *one* $|\pi N^*\rangle$ channel along with the $|\pi N\rangle$ channel. On the other hand, it is desired to include as much of the $|\pi N^*\rangle$ behavior as possible. The $\langle\frac{3}{2}{}^\pm|$ and $\langle\frac{1}{2}{}^\pm|$ amplitudes are generally of comparable magnitude, and to ignore one in this calculation would be a possible but not satisfactory approximation. A unitary transformation applied to these two final states gives two new independent final states which are suitable as channels for the T matrix. Hopefully, such a transformation can be found which results in one channel having larger amplitudes than the other in the region of interest. In looking for such a transformation, it is useful to consider a nonrelativistic $N^*(1236)$. (For W less than a few GeV, the N^* does not have very much kinetic energy in the $|\pi N^*\rangle$ c.m. frame.) Since spin is a good quantum number for a nonrelativistic particle, there is another natural way to define two independent final states of given J and parity. Spin $\frac{3}{2}$ can couple to *two* different values of orbital angular momentum L, to give a specified J and parity.[34] Furthermore, as in nuclear physics, the presence of a "centrifugal barrier" inhibits transitions, and it is expected that amplitudes for transitions into the lower L state are greater in magnitude than amplitudes for transitions into the higher L state.

The unitary transformation that gives the L states in terms of the helicity states is given below. The relations in Jacob and Wick[32] are used, and the Clebsch-Gordan coefficients are evaluated explicitly. For parity $(-1)^{J+1/2}$ the higher L (denoted $L_{\max}$) coupling has $L=J+\frac{3}{2}$, while the lower L (denoted $L_{\min}$) coupling has $L=J-\frac{1}{2}$:

$$\begin{aligned} (4J+4)^{1/2}\langle J,L_{\max}{}^+| &= -(J-\tfrac{1}{2})^{1/2}\langle\tfrac{3}{2}{}^+| \\ &\quad+[3(J+\tfrac{3}{2})]^{1/2}\langle\tfrac{1}{2}{}^+|\,, \\ (4J+4)^{1/2}\langle J,L_{\min}{}^+| &= -[3(J+\tfrac{3}{2})]^{1/2}\langle\tfrac{3}{2}{}^+| \\ &\quad-(J-\tfrac{1}{2})^{1/2}\langle\tfrac{1}{2}{}^+|\,. \end{aligned} \tag{5.29}$$

[32] M. Jacob and G. C. Wick, Ann. Phys. (N. Y.) 7, 404 (1959).
[33] A. R. Edmonds, *Angular Momentum in Quantum Mechanics* (Princeton University Press, Princeton, N. J., 1957).
[34] Of course, if $J=\frac{1}{2}$ there is only one channel, which has $|\lambda_2|=\frac{1}{2}$.

TABLE I. Mixing angle, final-state enhancement factors [Eq. (7.6)], and subtraction points.

State	$\tan\varepsilon$[a] Mixing angle	Model I[b] g_{expt} (GeV)	Model I[b] M_s (GeV)	Model II[c] g_{expt} (GeV)	Model II[c] M_s (GeV)	g (GeV) for $M_s=m$
$\frac{3}{2}^+$, $\frac{3}{2}$ (1236)	0.00{d,e	19.8	0.77	24.0	0.72	8.2[f]
		13.2	0.85	16.1	0.82	
$\frac{3}{2}^-$, $\frac{1}{2}$ (1525)	−0.98	8.6	0.78	8.3	0.80	5.9
$\frac{5}{2}^-$, $\frac{1}{2}$ (1680)	+1.25	0.32	physical region	8.0	1.06	10.2
$\frac{5}{2}^+$, $\frac{1}{2}$ (1688)	+0.89	25.9	−0.29	8.0	0.99	8.8
$\frac{7}{2}^+$, $\frac{3}{2}$ (1950)	−1.26	15.5	0.41	15.8	0.39	9.5

[a] $\tan^2\varepsilon$ is obtained from Eqs. (3.37) and (3.38). The sign of ε is chosen to give the most consistent set of subtraction points in model II. For the $\frac{5}{2}^-$ and $\frac{5}{2}^+$ states, using the same final-state enhancement factor only the indicated choice of signs gives a ratio of resonant contributions consistent with photoproduction (Ref. 35). For the $\frac{3}{2}^-$ state both signs of ε give reasonable subtraction points, but $\varepsilon<0$ gives a better fit to the SLAC data (Fig. 10).
[b] Over-all normalization needed to fit the experimental integrated cross sections using Eq. (3.44).
[c] Over-all normalization needed to fit the experimental integrated cross sections using Eq. (3.43).
[d] Normalization from SLAC data (Fig. 9).
[e] Normalization from data of Fig. 4.
[f] This number as well as the listed subtraction points for the $\frac{3}{2}^+$, $\frac{3}{2}$ (1236) are obtained by integrating over the *real part* of the elastic phase shift. If an integral over the eigenphase shift is used, the corresponding value of $g(M_s=m)$ is 4.5 GeV.

The couplings for parity $(-1)^{J-1/2}$ (superscript minus) are $L=J+\frac{1}{2}$ and $J-\frac{3}{2}$:

$$\begin{aligned}(4J)^{1/2}\langle J,L_{\max}{}^-|&=[3(J-\tfrac{1}{2})]^{1/2}\langle\tfrac{3}{2}^-|\\&\quad-(J+\tfrac{3}{2})^{1/2}\langle\tfrac{1}{2}^-|\,,\\(4J)^{1/2}\langle J,L_{\min}{}^-|&=(J+\tfrac{3}{2})^{1/2}\langle\tfrac{3}{2}^-|\\&\quad+[3(J-\tfrac{1}{2})]^{1/2}\langle\tfrac{1}{2}^-|\,,\end{aligned}\tag{5.30}$$

where the parity states $\langle\lambda_2{}^\pm|$ are defined in (5.27).

Although L is not a good quantum number in the relativistic case, the unitary transformation given in (5.29) and (5.30) does *define* the two independent states $\langle J,L_{\max}{}^\pm|$ and $\langle J,L_{\min}{}^\pm|$, which can be used as channels for the T matrix. The results of this calculation showed that the amplitudes $\langle J,L_{\max}{}^\pm|T^J(W,k^2)|\lambda_1\lambda_k{}^\pm\rangle$ were generally an order of magnitude smaller than the $\langle J,L_{\min}{}^\pm|T^J(W,k^2)|\lambda_1\lambda_k{}^\pm\rangle$. As a result the $L_{\min}$ channel was included in this model while the $L_{\max}$ channel was ignored. Of course, for W greater than a few GeV, the N^* is relativistic and other channels such as $L_{\max}$, ρN, or πN^{**} may be important.

The final resonant multipole amplitudes within the framework of the present model are thus given by

$$\begin{aligned}A(W,k^2)_{\lambda_1\lambda_k}{}^{J\pi}=&[\langle\pi N^\pm|T^J(W,k^2)|\lambda_1\lambda_k{}^\pm\rangle^{\text{lhs}}\cos\varepsilon\\&+\langle\pi N^*L_{\min}{}^\pm|T^J(W,k^2)|\lambda_1\lambda_k{}^\pm\rangle^{\text{lhs}}\sin\varepsilon]/D^{J\pi}(W)\end{aligned}\tag{5.31}$$

for each of the initial parity states $|\lambda_1\lambda_k\rangle=|\frac{3}{2}^\pm\rangle$, $|\frac{1}{2}^\pm\rangle$, $|L^\pm\rangle$ defined in Eq. (5.28). The cross section expressed in terms of these amplitudes is [see I, Eq. (3.31) and Appendix C of this paper]

$$\begin{aligned}\left(\frac{d^2\sigma}{d\Omega_2 d\epsilon_2}\right)_{\text{lab}}=&\frac{\alpha^2\cos^2(\frac{1}{2}\theta)}{4\epsilon_1{}^2\sin^4(\frac{1}{2}\theta)}\sum_{J\pi}(J+\tfrac{1}{2})\left\{\frac{k^4}{k^{*4}}|A_c{}^{J\pi}|^2\right.\\&+\left[\frac{1}{2}\frac{k^2}{k^{*2}}+\frac{W^2}{m^2}\tan^2(\tfrac{1}{2}\theta)\right]\\&\left.\times[|A_{3/2}{}^{J\pi}|^2+|A_{1/2}{}^{J\pi}|^2]\right\}\left(\frac{m}{k^*W}\right).\end{aligned}\tag{5.32}$$

[The Coulomb and longitudinal matrix elements are related by $A_c=(k^*/k_0)A_L$; compare I, Eq. (3.20).]

Figures 5 and 6 show a comparison of the k^2 dependence of the two-channel cross section with the one-channel results from I for the 1525- and 1688-MeV resonance regions. The values of the mixing angles used are given in Table I. The magnitude is obtained from the phase-shift analyses and Eqs. (3.37)–(3.38), while the sign of ε is essentially chosen to give the most consistent set of subtraction points (see Sec. 7 and the caption to Table I). The curves are normalized to fit the data and the resulting normalization constants are compared with the theoretical calculations of $D^{J\pi}(W)$ in Sec. 7. The contribution of the s-wave resonance in the 1525-MeV region was found to be negligible (with this choice of parameters) when the relative strength was again adjusted to that determined in photoproduction[35,36] (see I). In the 1688-MeV resonance region, the relative contribution of the $\frac{5}{2}^-$ resonance to the $\frac{5}{2}^+$ was fit to the photoproduction value of 7%.[35] The contribution of the s-wave resonances which lie in this region is again negligible at all k^2 if their relative contribution is small in photoproduction, as seems to be the case.[35] (With the present choice of parameters, their relative contribution again decreases as a function of k^2 just as in I.)

Also shown in Figs. 5 and 6 is the pure threshold behavior[1]

$$\begin{aligned}\frac{d\sigma}{d\Omega_2}(J^\pi\leftarrow\tfrac{1}{2}^+)\cong&\frac{\alpha^2\cos^2(\frac{1}{2}\theta)}{4\epsilon_1{}^2\sin^4(\frac{1}{2}\theta)}\frac{1}{1+(2\epsilon_1/m)\sin^2(\frac{1}{2}\theta)}\\&\times\left\{\frac{k^4}{k^{*4}}+\frac{k_0{}^2}{k^{*2}}\left(\frac{J+\frac{1}{2}}{J-\frac{1}{2}}\right)\left(\frac{k^2}{2k^{*2}}+\frac{W^2}{m^2}\tan^2(\tfrac{1}{2}\theta)\right)\right\}\\&\times|a_J{}^c|^2(k^*)^{2J-1},\quad(J>\tfrac{1}{2})\end{aligned}\tag{5.33}$$

[35] R. L. Walker, Phys. Rev. (to be published); S. D. Ecklund and R. L. Walker, *ibid.* **159**, 1195 (1967).
[36] Y. C. Chau, Norman Dombey, and R. G. Moorhouse, Phys. Rev. **163**, 1632 (1967).

for normal parity transitions, again normalized to photoproduction. This determines the constant $a_J{}^c$.

The most interesting feature of these results is the similarity in the predictions of the k^2 dependence in the one- and two-channel calculations. The ratio $d\sigma_{\text{inel}}/d\sigma_{\text{el}}$ is predicted to flatten out for $k^2 \gtrsim 1$ GeV^2, while the ratio based only on threshold behavior continues to rise. The curvature away from the threshold behavior and the leveling off are clearly very model-dependent results. It is a little surprising that the one- and two-channel predictions agree so closely. These results will be discussed in detail in Sec. 7.

6. FURTHER CORRECTIONS TO THE THEORY

There are two further modifications of the theory which can and should be investigated. The first is the extension of the excitation mechanism for the $|\pi N\rangle$ channel used in I. For example, because of the similarity in the behavior of their form factors, one should really include the exchange of all of the N^*'s in discussing the large k^2 behavior of the N^* form factors themselves. Also, since there still remains the ambiguity over the high-l versus s-wave-dominant fits,[4] it is important to investigate the effects of the exchange of more massive particles. As a first attempt in this direction, the $N^*(1236)$ exchange graph has been included. Again, just the coupling of Eq. (5.1) has been retained. The resulting contribution to the $|\pi N\rangle$ excitation amplitude is

$$\begin{aligned}(2\omega_q E_1 E_2 \Omega^3/m^2)^{1/2}&\langle q p_2{}^{(-)}|J_\mu(0)\epsilon_\mu|p_1\rangle \\ &= -\gamma_{\pi(\pm,0)}(C_3/m_\pi)\bar{u}(p_2\lambda_2)\epsilon_\mu\gamma_5[k_\nu\gamma_\mu-(\gamma\cdot k)\delta_{\mu\nu}] \\ &\times[i(\gamma\cdot p_2-\gamma\cdot k)+M]^{-1}\{q_\nu+(i/3M) \\ &\times[\gamma_\nu(p_2-k)\cdot q-(\gamma\cdot q)(p_2-k)_\nu]+(2/3M^2)(p_2-k)_\nu \\ &\times(p_2-k)\cdot q-\tfrac{1}{3}\gamma_\nu(\gamma\cdot q)\}u(p_1\lambda_1). \quad (6.1)\end{aligned}$$

The coupling constants are determined from Eqs. (5.2)–(5.8). This amplitude can be expanded in the invariants of I and added to the amplitudes there. In fact, the calculation of I was redone using a procedure similar to that described in Appendix B. This provided a numerical check of the results presented in I and a simple means for including more complicated graphs.

The resulting curves for electron excitation of the $N^*(1236)$ resonance with and without $N^*(1236)$ exchange (models II and I) are shown in Figs. 4 and 9. The transverse contributions are indistinguishable while there is a slight effect on the Coulomb form factor. The modification of the coupled-channel calculation due to the inclusion of $N^*(1236)$ exchange in the $|\pi N\rangle$ channel is shown in Figs. 5 and 6. The change in k^2 dependence is not significant, and the high-l versus s-wave-dominant ambiguity still remains.

This $N^*(1236)$ exchange is included in the curves marked model II in Figs. 4–12 and in the normalization constants and multipole ratios at photoproduction discussed as model II in Sec. 7.

It is also of interest to investigate the effect of possible alternative fits to the *elastic* nucleon form factors on the present calculation of the inelastic form factors. The elastic form factors enter through the excitation graphs. In the work discussed so far, the following scaling laws have been assumed:

$$G_{Ep}=\frac{G_{Mp}}{\mu_p}=\frac{G_{Mn}}{\mu_n}=-\frac{4m^2}{k^2}\frac{G_{En}}{\mu_n}. \quad (6.2)$$

In discussing the theoretical and experimental values of $d\sigma_{\text{in}}/d\sigma_{\text{el}}$ the actual *form* of G_{Ep} is not needed. These scaling laws imply that

$$F_1\equiv[G_E+(k^2/4m^2)G_M]/(1+k^2/4m^2) \quad (6.3)$$

vanishes for the neutron. It is convenient to examine the validity of the scaling law in terms of the empirical dipole fit to G_{Mp}/μ_p,

$$G_{Mp}/\mu_p=[1+k^2/0.71\ \text{GeV}^2]^{-2}. \quad (6.4)$$

This dipole fit to G_{Mp} has been verified with considerable accuracy up to $k^2\approx 25$ GeV,[2] the fit for G_{Ep} up to $k^2\approx 4$ GeV^2, the fit for G_{Mn} up to $k^2\approx 1.2$ GeV^2, and the situation with regards to G_{En} is still very much up in the air.[37] There is some evidence that the fit to G_{En} given in Eq. (6.2) gives slightly too large a value of $|G_{En}|$ at $k^2\approx 4$ GeV^2, the highest value at which it has has been measured. The scaling law in Eq. (6.2) also has the rather interesting feature that at large k^2 G_{En} is the dominant form factor.[38] An alternative scaling law, consistent with existing data, is

$$G_{En}=-\frac{k^2/4m^2}{1+k^2/4m^2}G_{Mn}. \quad (6.5)$$

The curves for model II shown in Figs. 4, 10, and 11 have been recomputed using Eq. (6.5). In all cases there is no appreciable change for $k^2 \lesssim 1$ GeV^2. For the 3-3 resonance the transverse cross section is increased slightly for $k^2>1$ GeV^2, the maximum increase being 15% at $k^2=5$ GeV^2. The Coulomb cross section is somewhat more sensitive to the change in G_{En}, but its general shape and magnitude relative to the transverse are not significantly changed. In the 1525-MeV region the cross section is increased for $k^2>1$ GeV^2, with the increase reaching 25% at $k^2=5$ GeV^2. For the 1688 region there is no change below 2 GeV^2, but then the cross section decreases, the change being 40% at $k^2=5$ GeV^2. Thus, even at large momentum transfers none of the curves are significantly altered, and a comparison of the present theory with experiment cannot distinguish between the scaling laws in (6.5) and (6.2).

[37] G. Weber, in *Proceedings of the International Symposium on Electron and Photon Interactions at High Energies, SLAC, 1967* (National Bureau of Standards, Springfield, Va., 1968), p. 59; R. E. Taylor, *ibid.*, p. 78.

[38] We wish to thank Dr. D. Silverman for a discussion of these points.

7. COMPARISON WITH EXPERIMENT

This section presents a comparison of the theory with all existing data on the inelastic form factors for the various nucleon resonances. A comparison is made with both the previous calculations of I (referred to as model I) and with the present coupled-channel calculations including $N^*(1236)$ exchange in the $|\pi N\rangle$ channel (referred to as model II). In making this comparison, a value is needed for the parameter β defined in I:

$$\beta=-\frac{g_{\omega\pi\gamma}g_{\omega NN}}{\frac{1}{2}g_{\pi N}F_2{}^V(0)}\cong-(\sqrt{10})\frac{g_{\omega\pi\gamma}}{|g_{\omega\pi\gamma}|}\frac{g_{\omega NN}}{g_{\pi N}}. \quad (7.1)$$

On the basis of the over-all comparison between theory and experiment a single value

$$\beta=-6 \quad (7.2)$$

was chosen. This number is very close to the other independent determinations of this quantity (see I; in particular I, Table II), and slightly less than the value $\beta=-8.2$ used in I. The sign is again crucial since it is necessary to add amplitudes. With this choice of sign, it is the high-l resonances which dominate the inelastic spectrum.[4] For all the isobars except the $N^*(1236)$ a comparison will be made directly with the ratio of inelastic to elastic cross section as a function of k^2 at a given electron scattering angle since there is as yet no experimental separation of the transverse and Coulomb contributions. The inelastic cross section is defined by

$$\frac{d\sigma_{\text{in}}}{d\Omega_2}\equiv\int_{\text{over resonance}}\left[\frac{d^2\sigma}{d\Omega_2 d\epsilon_2}\right]_{\epsilon_1,\theta}d\epsilon_2, \quad (7.3)$$

$$\frac{d\sigma_{\text{in}}}{d\Omega_2}=\frac{\sigma_M}{1+(2\epsilon_1/m)\sin^2(\frac{1}{2}\theta)}\times\int_{\text{over resonance}}\left[\frac{1}{\sigma_M}\frac{d^2\sigma}{d\Omega_2 d\epsilon_2}\right]_{\epsilon_1,\theta}\left(\frac{W}{m}\right)dW, \quad (7.4)$$

with

$$\sigma_M\equiv\alpha^2\cos^2(\tfrac{1}{2}\theta)/4\epsilon_1{}^2\sin^4(\tfrac{1}{2}\theta) \quad (7.5)$$

[see I, Eq. (3.33)]. The k^2 associated with $d\sigma_{\text{in}}$ is that evaluated on the resonance peak $W=W_R$. The actual value of the elastic form factor cancels in the theoretical expressions for the ratio $d\sigma_{\text{in}}/d\sigma_{\text{el}}$, and all that is needed is the scaling law for the elastic form factors. Equation (6.2) was used for this. (The dependence of the results on the assumed form of G_{En} is discussed in Sec. 6.) For the $N^*(1236)$ a separation of transverse and Coulomb contributions has been carried out and a comparison is made of the ratios to $G_{Ep}{}^2$. To evaluate the experimental values of this ratio, the fit (6.4) was used. The values of ε used in the coupled-channel calculation are given in Table I and discussed in Sec. 5. All the coupling constants have been discussed in the text.

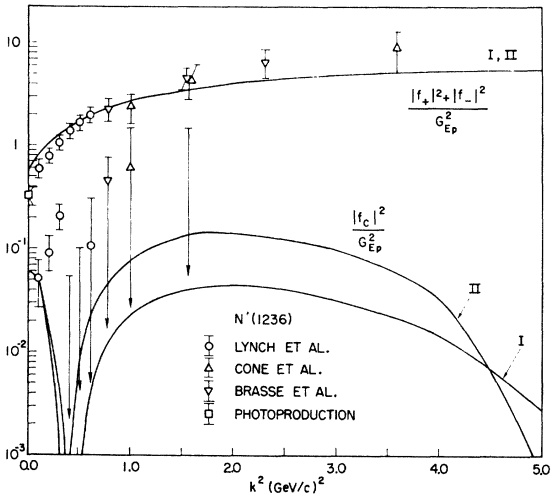

FIG. 4. $[|f_+|^2+|f_-|^2]/G_{Ep}{}^2$ and $|f_c|^2/G_{Ep}{}^2$ for the $\frac{3}{2}^+$, $\frac{3}{2}$ (1236) resonance. The predictions of models I and II (defined in the text) are indicated. The experimental points are from Refs. 39–41. At the highest k^2 point from both Cone *et al.* and Brasse *et al.*, the cross section has been assumed to be entirely transverse. The point at $k^2=0$ is determined from the photoproduction data in Refs. 35 and 40 by means of Eq. (1.2). (See also Ref. 1.)

In all of the comparisons between theory and experiment the theoretical curves have been normalized to fit the data. It is the k^2 dependence which is then predicted. The values of the resulting normalization constants are discussed at the end of this section.

Figures 4–7 give the comparison with the data of Lynch *et al.* (Stanford)[39] and Cone *et al.* (CEA)[40] as well as with the new data of Brasse *et al.* (DESY).[41] For the $\frac{3}{2}^+$, $\frac{3}{2}$ (1236) resonance the Stanford group was able to separate the Coulomb and transverse contributions, and thus in Fig. 4 the predictions for these two contributions are plotted separately. The CEA and DESY data permit estimates of upper limits for the Coulomb contribution. Stanford and DESY give the peak height of the cross section, while for the comparison given in Fig. 4 it is necessary to have the cross section integrated over the resonance. The values of the integrated form factors given in Fig. 4 were obtained by assuming that the relative background contribution is constant over k^2 and equal to the value at photoproduction.[42] The resulting error in the transverse contribution should be fairly small, but it is not at all clear how much of the measured Coulomb contribution is due to the resonance itself and how much is due to the nonresonant background. Thus, the Coulomb points should probably

[39] H. L. Lynch, J. V. Allaby, and D. M. Ritson, Phys. Rev. **164**, 1635 (1967).

[40] A. A. Cone, K. W. Chen, J. R. Dunning, Jr., G. Hartwig, Norman Ramsey, J. K. Walker, and Richard Wilson, Phys. Rev. **156**, 1490 (1967); **163**, 1854(E) (1967).

[41] F. W. Brasse, J. Engler, E. Ganssauge, and M. Schweizer, Nuovo Cimento **55A**, 679 (1968).

[42] In I, the errors on our treatment of the Stanford data due to the uncertainty in the background subtraction and integration over the resonance were understated.

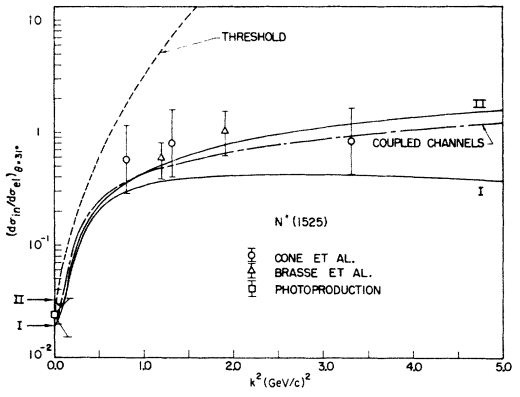

FIG. 5. Ratio of the resonant inelastic to the elastic cross section, $d\sigma_{\rm in}/d\sigma_{\rm el}$, at 31° for the 1525-MeV region. $d\sigma_{\rm in}/d\Omega_2$ is given in Eq. (1.1). $d\sigma_{\rm el}/d\Omega_2$ is given by

$$\left(\frac{d\sigma_{\rm el}}{d\Omega_2}\right)_{\rm lab}=\frac{\alpha^2\cos^2(\frac{1}{2}\theta)}{4\epsilon_1^2\sin^4(\frac{1}{2}\theta)\,[1+(2\epsilon_1/m)\sin^2(\frac{1}{2}\theta)]}\times\{[G_{Ep}{}^2+(k^2/4m^2)G_{Mp}{}^2]/(1+k^2/4m^2)+[(k^2/2m^2)\tan^2(\tfrac{1}{2}\theta)\,G_{Mp}{}^2]\}.$$

The predictions of model I, model II, the coupled-channel calculation (model II without N^* exchange in the $|\pi N\rangle$ channel), and the pure-threshold behavior [Eq. (5.33)] are shown. The point at $k^2=0$ is determined from the photoproduction data in Refs. 35 and 40.

be considered only as order-of-magnitude estimates. The fit to the transverse data is quite good, and the relative magnitude of the Coulomb contribution given by the model is consistent with the experimental upper limits. The prediction of a diffraction minimum in the Coulomb cross section is interesting.

Figures 5–7 give a comparison of the ratio $d\sigma_{\rm in}/d\sigma_{\rm el}$ with the measurements of Cone *et al.*[40] at 31° for the 1525-, 1688-, and 1950-MeV resonance region. The normalizations of the theoretical curves in these figures are determined from the fit to the preliminary SLAC data (see Figs. 10–12). The data of Brasse *et al.*[41] are also included in Figs. 5 and 6. For these data the resonant part of the cross section has been estimated by the present authors with a procedure similar to that of the CEA group,[40] and use has been made of the predicted ratio of Coulomb to transverse excitation to extrapolate the data from 47.4° to 31°. The quoted error is due almost entirely to the uncertainty in estimating the resonant part. From Walker's analysis of single-pion photoproduction,[35] the cross section at $k^2=0$ in Fig. 6 is estimated to be 93% $\frac{5}{2}^+$, $\frac{1}{2}$ (1688) and 7% $\frac{5}{2}^-$, $\frac{1}{2}$ (1680). Note that the fit does not fall fast enough at photoproduction. The relative contribution of the *s*-wave resonances which are present in the 1525 and 1688 regions is small at photoproduction[2,35,36] and *decreases* with increasing k^2 for the present choice of parameters in the theory. Their contribution is therefore negligible in Figs. 5 and 6. The electron scattering points in Fig. 7 are upper limits.

Extensive experiments on inelastic electron scattering are being performed at SLAC, and some preliminary results are now available.[6] The measurements taken so far do not permit any separation of Coulomb and transverse cross sections. The extraction of the resonance cross section from the data is by no means straightforward, particularly for the higher resonances, as we have indicated. The most ambitious procedure developed so far is that of Mo used in the preliminary analysis of the SLAC data.[6,43] In his fit to the data he employs four Breit-Wigner shapes plus a polynomial background term. For the $N^*(1236)$ the width is given a *p*-wave momentum dependence and thus the shape is asymmetric. The locations and widths of the four resonances are free parameters (as well as the heights of the resonances). The results of his least-squares fits show that the integrated cross sections are insensitive to the order of the poly-

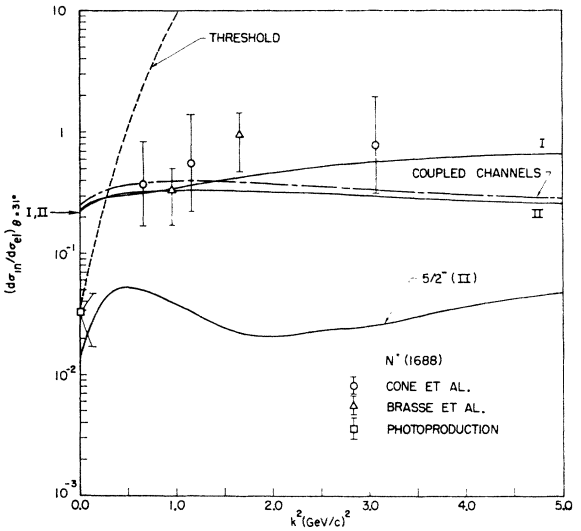

FIG. 6. Same as Fig. 5 for the 1688-MeV region. The contribution of the $\frac{5}{2}^-$, $\frac{1}{2}$ (1680) state is shown for model II; for all values of k^2 considered, the cross section is dominated by the $\frac{5}{2}^+$, $\frac{1}{2}$ (1688) state.

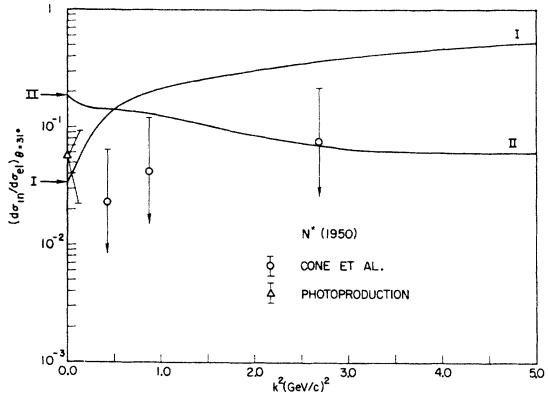

FIG. 7. $d\sigma_{\rm in}/d\sigma_{\rm el}$ at 31° for the 1950-MeV resonance. The electron scattering points are upper limits from Ref. 40. The point at $k^2=0$ is determined from the photoproduction data in Ref. 35.

[43] L. Mo (private communication).

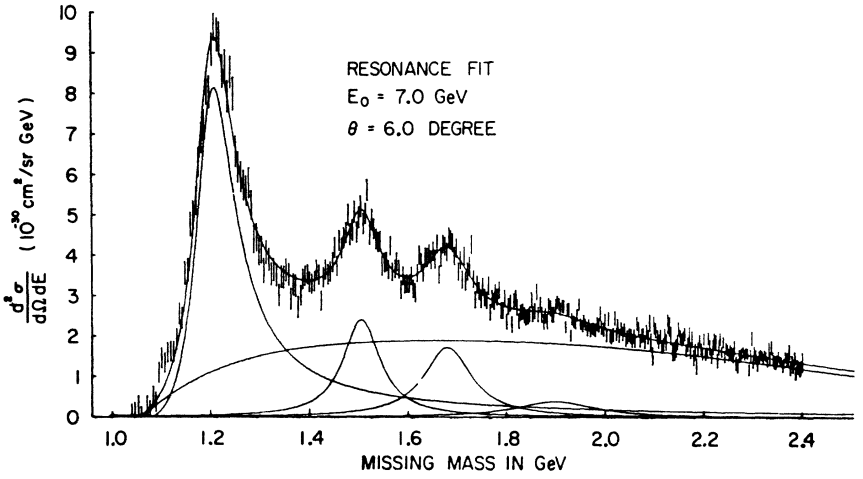

FIG. 8. The SLAC experimental inelastic spectrum at $\epsilon_1 = 7$ GeV, $\theta = 6°$, resolved into Breit-Wigner resonances by the fitting procedure discussed in the text. This figure is from Ref. 6.

nomial assumed for the background. A typical decomposition into resonances and background is shown in Fig. 8.[6] The data of all the inelastic electron scattering experiments should be analyzed at least as extensively as the SLAC data if accurate results are to be obtained for the integrated resonance cross section. Figures 9–12 compare the predictions for the ratio of inelastic to elastic cross section at 6° with the preliminary SLAC data. From Fig. 9 it is seen that the fit to the k^2 dependence of the 3-3 data is excellent. The normalization based on the Stanford, CEA, and DESY data, however, is low by $\sim$40%. This discrepancy is presumably due in part to the different methods employed for extracting resonance parameters from the data. The SLAC procedure is certainly the most consistent and thorough. It is also partly due to the large tail on the high-energy side of the $N^*(1236)$ in the SLAC fit. For example, there is a 20% contribution to the integrated area coming from the region $2 \leq W \leq 4$ GeV in Mo's analysis.[43] The k^2 dependence of the prediction for the 1525 resonance region shown in Fig. 10 is also excellent. From Fig. 5 it is seen that the predictions with the SLAC normalization lie somewhat below the CEA and DESY data. The difference in normalization for the 1525 region may again be due in part to the procedure used in estimating the resonant cross section. However, it should be emphasized that the cross section at 31° measures a different combination of the Coulomb and transverse form factors than does the cross section at 6°, and thus a further test of the model is involved in comparing these different sets of data. For the 1688 region shown in Fig. 11 the k^2 dependence is only fair. In particular, the theory is never able to get down to the photoproduction point. If just the electron scattering points are considered, however, the k^2 dependence is not bad. The preliminary SLAC results yield just one value for the 1950 resonance region as shown in Fig. 12 (the curves are normalized to this point). This gives results at 31° lying somewhat above the error bars on the CEA data (Fig. 7).

In addition to the k^2 dependence of the form factors, the predictions of the model for the shapes of the resonances (see Sec. 4) can be compared with experiment. The most direct comparison is with Mo's preliminary decomposition of the SLAC data shown in Fig. 8. Figure 13 shows the predicted spectrum for the same experimental conditions. The normalizations used in Fig. 13 correspond to the best fit to the SLAC data as shown in Figs. 9–12. Thus, the area under corresponding resonances is about the same in both figures. For the 3-3 resonance the widths are nearly identical. The average width at half-maximum for all the SLAC spectra is 105±10 MeV, which is in excellent agreement with the 105 MeV predicted by the model. But for the 1525 and 1688 regions the SLAC widths are considerably smaller. The averages are 77±14 and 102±10 MeV, respectively. These widths are about half the predicted

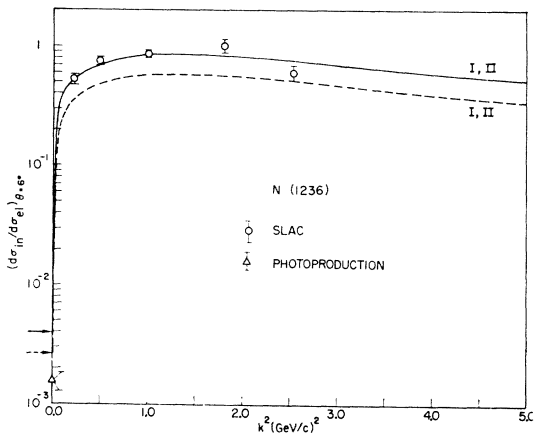

FIG. 9. $d\sigma_{in}/d\sigma_{el}$ at 6° for the $\frac{3}{2}^+$, $\frac{3}{2}$ (1236) resonance. The experimental points are the preliminary SLAC data (Ref. 6). The solid curve is normalized to these data. The dashed curve is normalized to the data of Fig. 4. In each of Figs. 9–11 the SLAC point at the smallest value of k^2 was measured at 4° rather than at 6°. From Eq. (1.1) and the form of $d\sigma_{el}/d\Omega_2$ (see the caption of Fig. 5) it is seen that the variation in $d\sigma_{in}/d\sigma_{el}$ between 4° and 6° is much smaller than the experimental error in all three cases.

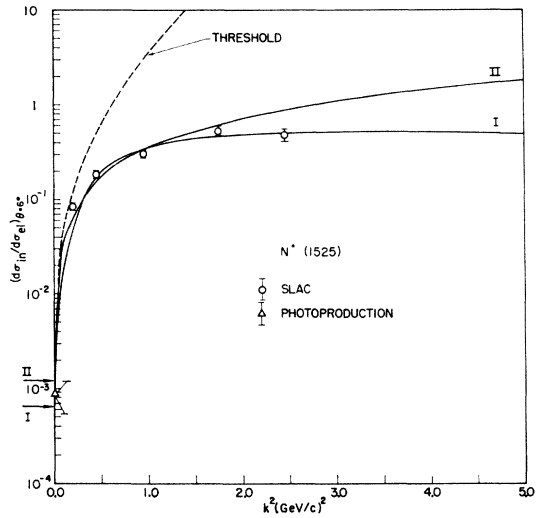

FIG. 10. $d\sigma_{\rm in}/d\sigma_{\rm el}$ at 6° for the 1525-MeV region. Also shown is the pure threshold behavior [Eq. (5.33)]. Experimental points are from Ref. 6.

values obtained from Fig. 2. They are also substantially smaller than the widths found in π-N scattering. Cone *et al.*, however, assumed much larger widths in their analysis[40]: 140 MeV for the 1525 region and 145 MeV for the 1688 region. This may explain in part why the integrated CEA values are larger than the SLAC values for the 1525 region. There is also some evidence that different fitting procedures can yield somewhat different widths.[6]

Another point of comparison is the location of the maximum of the cross section. For the 3-3 resonance the average of all the SLAC spectra is 1219±10 MeV. This is in very good agreement with the predicted value of 1222 MeV (Fig. 2). For the second and third resonance in the SLAC spectra, the average peak locations

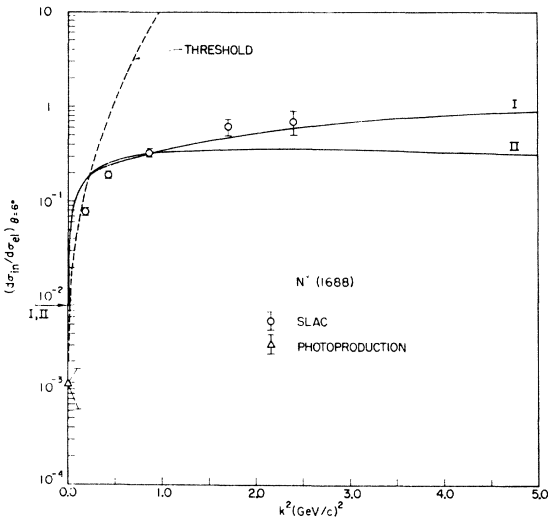

FIG. 11. Same as Fig. 10 expect for the 1688-MeV region.

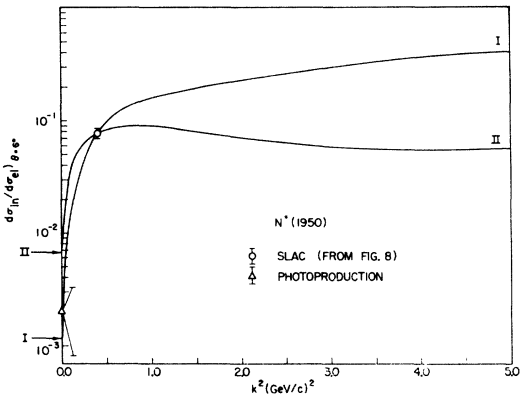

FIG. 12. $d\sigma_{\rm in}/d\sigma_{\rm el}$ at 6° for the 1950-MeV region. The curves are normalized to the integrated area under the fourth Breit-Wigner curve in Fig. 8. The error shown is the statistical error in the fitting procedure used in Fig. 8 (Ref. 43).

are 1503±10 and 1691±10 MeV, respectively. These are considerably higher than the predicted values (Fig. 2) for the $\frac{3}{2}^-$, $\frac{1}{2}$ (1525) and $\frac{5}{2}^+$, $\frac{1}{2}$ (1688) or $\frac{5}{2}^-$, $\frac{1}{2}$ (1680) resonances. However, as mentioned earlier, predictions of shapes and spectra are strongly dependent on the particular model used in the calculation. Thus, the discrepancies here are perhaps not so surprising. Also, one should note that the disagreement would probably be much worse for the alternative $\beta=+4.0$ s-wave-dominant solution discussed in I. In this solution the inelastic cross sections away from $k^2=0$ are dominated by the $I=\frac{1}{2}$ s-wave resonances (at 1550 and 1710 MeV). Thus, to reproduce the SLAC results it would be necessary to get two sharp peaks from one channel. Because these two resonances overlap considerably in π-N scattering ($\Gamma_{1550}=130$ MeV and $\Gamma_{1710}=300$ MeV), it seems highly unlikely that this could be the case.

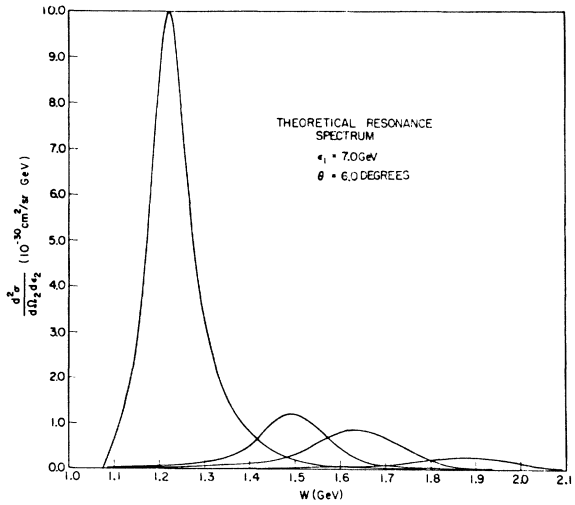

FIG. 13. The predicted resonance spectrum at $\epsilon_1=7$ GeV, $\theta=6°$, to be compared with Fig. 8. Note that this spectrum corresponds to values of k^2 in the "threshold" region ($k^2=0.49$ GeV^2 at the 3-3 peak), and consequently the second and third resonances are still dominated by the 3-3 resonance.

TABLE II. Photoproduction amplitudes.

State	Ratio	Experiment		Model I		Model II	
		Walker[a]	Moorhouse *et al.*[b]	$\beta=-6$	$\beta=-4$	$\beta=-6$	$\beta=-4$
$\frac{3}{2}^+$, $\frac{3}{2}$ (1236)	E_1^+/M_1^+	-0.04 ± 0.08		-0.34	-0.25	-0.38	-0.27
$\frac{3}{2}^-$, $\frac{1}{2}$ (1525)	M_2^-/E_2^-	$+0.48\pm0.2$	$+0.34$	-0.49	$+0.03$	$+0.11$	$+0.27$
$\frac{5}{2}^-$, $\frac{1}{2}$ (1680)	E_2^+/M_2^+	$-0.5\ \pm0.5$		-0.33	-0.42	$+4.0$	$+0.85$
$\frac{5}{2}^+$, $\frac{1}{2}$ (1688)	M_3^-/E_3^-	$+0.5\ \pm0.3$		-0.07	$+0.07$	-0.07	-0.04
$\frac{7}{2}^+$, $\frac{3}{2}$ (1950)	E_3^+/M_3^+			$+1.5$	-1.05	$+0.38$	$+0.49$

[a] Reference 35. [b] Reference 36.

Because of these complexities it has not yet been possible to carry out a convincing coupled-channel calculation in the s-wave-dominant case. *The fact that the simple model of one nonzero eigenphase shift together with negative β produces qualitatively reasonable spectra at all k^2 is the strongest reason of believing that the high-l dominant solution discussed here is correct.*

The model predicts ratios of multipole amplitudes for a given resonance at all values of k^2. At $k^2=0$ these ratios can be compared with the experimental values determined from the various phenomenological analyses of photoproduction.[35,36] The comparison is shown in Table II. Note that the value $\beta=-4$ gives a much more reasonable set of ratios while not significantly changing the fit to the form factors. Also, the coupled-channel calculation greatly improves the agreement for the $\frac{3}{2}^-$, $\frac{1}{2}$ (1525) resonance, and one therefore begins to get a glimmer of a quantitative theory of the first *two* nucleon resonances. The discrepancies for the $\frac{5}{2}^-$, $\frac{1}{2}$ (1680) and $\frac{5}{2}^+$, $\frac{1}{2}$ (1688) resonances are not removed, and the model does not appear to be a detailed theory of resonant photoproduction in this region.

Finally, we come to the determination of the subtraction point M_s in the expression for $D(W)$ [see Eq. (4.6)]. M_s is determined from the over-all normalization needed to fit the experimental integrated cross sections using the final-state enhancement factor

$$g\equiv\int_{\text{res}}\frac{1}{|D(W)|^2}dW\simeq\frac{2\pi}{\Gamma}\frac{1}{|\mathrm{Re}'D(W_R)|^2}. \quad (7.6)$$

The experimental values of these factors are given in Table I for both model II [Eq. (3.43)] and model I [Eq. (3.44)]. In determining M_s from the normalization the area has been approximated as on the right-hand side of Eq. (7.6). The resulting values of M_s are given in Table I. The values for the $\frac{3}{2}^-$, $\frac{1}{2}$ (1525), $\frac{5}{2}^+$, $\frac{1}{2}$ (1688), $\frac{5}{2}^-$, $\frac{1}{2}$ (1680), and $\frac{7}{2}^+$, $\frac{3}{2}$ (1950) resonances are all very similar in the coupled-channel calculation for the fit to the data. It is interesting that the values of M_s are all near the nucleon mass. It is clear by comparing with the values of M_s obtained in model I that the major accomplishment of the coupled-channel calculation is to give a uniform subtraction point. The implication of this fact will be discussed in Sec. 8. It is merely worth noting in passing that if one were to take it as a principle that

$$M_s=m \quad (7.7)$$

as in the Chew-Low theory of the $N^*(1236)$ resonance,[28] then all the relative and absolute cross sections of the resonances considered here agree with experiment to within approximately a factor of 2.[44]

8. SUMMARY AND CONCLUSIONS

In I a simple relativistic model was developed to obtain some predictions for the form factors for electron excitation of the nucleon resonances. The predictions for the k^2 dependence of these form factors are in remarkably good agreement with the recent SLAC data. In the present paper an attempt has been made to develop the model sufficiently so that one has at least the beginning of a theory. The principal modification is a coupled-channel calculation retaining $|\pi N\rangle$ and $|\pi N^*(1236)\rangle$ and assuming that only one particular linear combination, or one eigenphase shift, is resonant (the eigenphase shifts extracted from the π-N scattering data under this assumption all show a very nice resonant behavior.) This leads to the expressions (5.31) and (5.32). The final-state enhancement factor is expressed in terms of an integral over the *real* eigenphase shift [Eqs. (3.48) and (3.49)]. The magnitude of the mixing angle is obtained from the branching ratios of the resonance into the two channels [Eqs. (3.37) and (3.38)]. The *sign* of ϵ is essentially chosen to give the most uniform set of subtraction points (Table I). A covariant gauge-invariant model for excitation of the $|\pi N^*(1236)\rangle$ channel has been developed using the generalized Feynman amplitudes shown in Fig. 3 and the appropriate multipoles have been projected from this amplitude. The k^2 dependence of the ratio $d\sigma_{\text{in}}/d\sigma_{\text{el}}$ in the coupled-channel calculation is very similar to that obtained in model I for the 1525 and 1688 resonance regions. Additional modifications of the theory which have been investigated are the inclusion of the $N^*(1236)$ exchange graph in the excitation amplitude

[44] This factor can be somewhat larger for the $N^*(1236)$, depending on just how one treats the normalization to the experimental data and the inelastic contribution to the final-state enhancement factor. See Table I.

for the $|\pi N\rangle$ channel and the effect of varying the scaling law for the elastic form factors.

The k^2 dependence of this more detailed calculation (model II) is in excellent agreement with the SLAC electron scattering results for the $\frac{3}{2}^+$, $\frac{3}{2}$ (1236) and $\frac{3}{2}^-$, $\frac{1}{2}$ (1525) resonances. There are slight normalization differences between the SLAC results and the previous results, and the theoretical curve in Fig. 9 does not come down to the photoproduction point. One reason for this is that it is difficult to extract the resonant contribution from the total inelastic electron scattering cross section and different procedures can lead to somewhat different results (for example, all the points in Fig. 4 were obtained by just assuming that the relative nonresonant background is the same as in photoproduction). The most ambitious program for extracting resonance parameters is that of Mo and the SLAC group and therefore the SLAC data for the resonant cross sections are the most internally consistent. The photoproduction point at $k^2=0$ always comes from a *completely different experiment* with different attendant backgrounds and uncertainties and this must always be kept in mind when extrapolating the electron scattering cross sections to the measured photoproduction value. The comparison with the SLAC electron scattering points for the $\frac{5}{2}^+$, $\frac{1}{2}$ (1688), $\frac{5}{2}^-$, $\frac{1}{2}$ (1680) resonance region is again quite good. The one serious problem for the theory here is that it does not come down far enough at photoproduction. As $k^2\to 0$ at a fixed θ one has from Eqs. (1.1) and (1.2)

$$\frac{d\sigma_{\text{in}}}{d\sigma_{\text{el}}} \underset{k^2\to 0}{\longrightarrow} \left[\frac{k^4}{k^{*4}}|f_c|^2+\left(\frac{k^2}{2k^{*2}}+\frac{W_R^2}{m^2}\tan^2(\tfrac{1}{2}\theta)\right)\times(|f_+|^2+|f_-|^2)\right], \quad (8.1)$$

$$\frac{d\sigma_{\text{in}}}{d\sigma_{\text{el}}} \underset{k^2=0}{\longrightarrow} \tan^2(\tfrac{1}{2}\theta)\frac{W_R^2-m^2}{m^2}\frac{m}{4\pi^2\alpha}\times\int_{\text{lab; over resonance}}\sigma_\gamma(\omega)d\omega. \quad (8.2)$$

The contribution at $k^2=0$ thus comes entirely from the transverse form factors. As k^2 increases from zero, the quantity k^2/k^{*2} quickly approaches 1 (it varies from 0.42 to 1.0 for all the electron scattering points discussed), and for small scattering angles the Coulomb scattering can make a major contribution. Thus, existing electron scattering results and the photoproduction point at $k^2=0$ are still testing different aspects of the theory in the 1525- and 1688-MeV resonance regions where the Coulomb contribution is important. The relative Coulomb contributions in these resonance regions in model II are qualitatively similar to those shown in I—Figs. 10 and 11. In the 1688 region, $|f_c|^2$ is a factor of 2 larger than $|f_+|^2+|f_-|^2$ except for $0\lesssim k^2\lesssim 0.7$ GeV^2, where the transverse dominates. This is presumably the reason that the present theory is able to fit the electron scattering points in this region and yet not get down to photoproduction. For the 1525-MeV resonance, $|f_c|^2$ shows a diffraction minimum as in I, only now at a somewhat larger value of $k^2\cong 1$ GeV^2. It dominates the transverse both at $k^2=0$ and $k^2\gtrsim 4$ GeV^2.

It is clear from Figs. 7, 8, and 12 that any comparison between theory and experiment for the $\frac{7}{2}^+$, $\frac{3}{2}$ (1950) resonance is inconclusive.

The most striking feature of the ratios $d\sigma_{\text{in}}/d\sigma_{\text{el}}$ is that they all level off with k^2 as soon as one gets away from the "threshold" region [the pure threshold behavior for normal parity transitions given by Eq. (5.33) is indicated on the appropriate figures]. The curvature away from the threshold values, the leveling off, and the region in k^2 where this occurs are, of course, the main predictions of the present model. It is surprising that such a simple theory in terms of relatively low-mass particles in the exchange channels can give a representation of the data to such large values of k^2.

Another striking feature of the ratios $d\sigma_{\text{in}}/d\sigma_{\text{el}}$ is that they *all level off at a value very close to 1.* Because the eigenphase shift appears to go to $\frac{1}{2}\pi$ as $W\to\infty$, one is forced to make a subtraction at some point $W=M_s$ in the final-state enhancement factor [Eqs. (3.48)–(3.49) and (4.6)–(4.7)] and can therefore say nothing *a priori* about the absolute normalization (without a more detailed theory of the strong interactions). Therefore, the theoretical curves in each resonance region are simply normalized to the experimental data. It is clear from Table I, however, that the resulting subtraction points are very similar and very close to the nucleon mass. From Fig. 2 it is seen that the final-state enhancement factors calculated with $M_s=m$ are also very similar. Indeed, the area under these curves differs from their mean by at most 50%. If the area were the same, then from Eqs. (5.31) and (5.32) it would follow that for resonances i and j at fixed k^2,

$$d\sigma_{\text{in}}(i)/d\sigma_{\text{in}}(j)\cong[d\sigma_{\text{in}}(i)/d\sigma_{\text{in}}(j)]^{\text{lhs}}. \quad (8.3)$$

Thus if we assume the same subtraction point $M_s\cong m$, then the ratio of the resonant cross sections is the same as the ratio of excitation cross sections. In fact, from Table I this is seen to hold to about a factor of 2.[44] Furthermore, if one says in addition that the dynamics are such that $M_s=m$ as in the Chew-Low static theory of the $N^*(1236)$, then the *absolute magnitude* of each of the resonance cross sections discussed here is given correctly to about a factor of 2.[44]

The predicted and experimental transverse multipole ratios at $k^2=0$ are compared in Table II. It is clear that these ratios are much more sensitive to the details of the model than $d\sigma_{\text{in}}/d\sigma_{\text{el}}$. For the $\frac{3}{2}^+$ (1236) and $\frac{3}{2}^-$ (1525) one is on the verge of having a quantitative theory of the electromagnetic properties. The model does not give a good representation of photoproduction in the 1688-MeV resonance region, however.

Finally, additional theoretical and experimental work is clearly called for. On the theoretical side one would like an enlarged coupled-channel calculation, particularly for the higher nucleon resonances, a more detailed solution to the coupled Omnès equations than the simple resonance approximation used here, and a better treatment of the excitation mechanism including the exchange of the higher N^*'s themselves and of vector mesons with both the charge and magnetic couplings retained. On the experimental side, it is crucial to have a determination of the dominant multipole contribution in the resonance region as a function of k^2 to decide once and for all between the high-l and s-wave-dominant solutions. In addition, a separation of Coulomb and transverse contributions, particularly in the 1525- and 1688-MeV resonance regions, will provide a much more stringent test of the theory. The *relative* Coulomb and transverse contributions can show very interesting behavior (see I) while $d\sigma_{\text{in}}$, which is the sum of the squares of these contributions, is a very smooth function of k^2. Indeed the inelastic Coulomb form factors may be expected to show diffraction minima in many cases (see, for example, Fig. 4) even though none appear in the elastic case. The most severe test for any theory (and experiment) will be to get the resonant multipole ratios as a function of k^2.

ACKNOWLEDGMENTS

The authors would like to thank R. Taylor and the members of SLAC Group A for many valuable discussions. In particular, they are very much indebted to L. Mo for discussions of the analysis of the experimental results.

APPENDIX A

The pole terms $A^{(i)}(W, k^2, k\cdot q)$ calculated from the graphs in Fig. 3 as discussed in Sec. 5 are given below. $A^{(1)}\cdots A^{(9)}$ are denoted by $A\cdots I$.

$$
\begin{aligned}
A&=a_1F_1{}^p(k^2)[(p_1+k)^2+m^2]^{-1}+a_1F_3(k^2)\\
&\qquad\times[(p_1-q)^2+M^2]^{-1},\\
B&=-(1/k\cdot q)a_1F_1{}^p(k^2)[(p_1+k)^2+m^2]^{-1}\\
&\quad-(1/k\cdot q)a_1F_3(k^2)[(p_1-q)^2+M^2]^{-1},\\
C&=-a_1F_2{}^p(k^2)[(p_1+k)^2+m^2]^{-1},\\
D&=-a_1F_2{}^p(k^2)[(p_1+k^2)+m^2]^{-1},\\
E&=(1/k\cdot q)a_2F_\pi(k^2)[(q-k)^2+m_\pi{}^2]^{-1},\\
F&=-2a_2F_\pi(k^2)[(q-k)^2+m_\pi{}^2]^{-1}-a_3[C_3(k^2)/m_\pi]\\
&\qquad\times[(p_1-q)^2+m^2]^{-1}+\tfrac{2}{3}a_1F_3(k^2)\\
&\qquad\times[(p_1-q)^2+M^2]^{-1},\\
G&=a_3[C_3(k^2)/m_\pi][(p_1-q)^2+m^2]^{-1}\\
&\quad-\tfrac{2}{3}a_1F_3(k^2)[(p_1-q)^2+M^2]^{-1},\\
H&=-a_2F_\pi(k^2)[(q-k)^2+m_\pi{}^2]^{-1},\\
I&=a_3[C_3(k^2)/m_\pi][(p_1-q)^2+m^2]^{-1}\\
&\quad-\tfrac{2}{3}a_1F_3(k^2)[(p_1-q)^2+M^2]^{-1},
\end{aligned}
\tag{A1}
$$

where for positive pion emission

$$a_1=\gamma_{\pi^+},\quad a_2=\gamma_{\pi^+},\quad a_3=-\sqrt{2}g_{\pi N},\quad F_3(k^2)=F_1{}^{n^*}(k^2);\tag{A2}$$

for neutral pion emission:

$$a_1=\gamma_{\pi^0},\quad a_2=0,\quad a_3=g_{\pi N},\quad F_3(k^2)=F_1{}^{p^*}(k^2);\tag{A3}$$

and for negative pion emission:

$$a_1=\gamma_{\pi^-},\quad a_2=-\gamma_{\pi^-},\quad a_3=0,\quad F_3(k^2)=2F_1{}^{N^{*++}}(k^2).\tag{A4}$$

The poles are easily expressed in terms of W, k^2, $k\cdot q$, and the masses:

$$
\begin{aligned}
&[(k-q)^2+m_\pi{}^2]^{-1}=(k^2-2k\cdot q)^{-1},\\
&[(p_1+k)^2+m^2]^{-1}=-(W^2-m^2)^{-1},\\
&[(p_1-q)^2+m^2]^{-1}=(2k\cdot q+W^2-M^2)^{-1},\\
&[(p_1-q)^2+M^2]^{-1}=(2k\cdot q+W^2-m^2)^{-1}.
\end{aligned}
\tag{A5}
$$

APPENDIX B

A Dirac spinor can be expressed as a Lorentz transformation operating on a two-component rest-frame spinor. Thus, the initial spinor in the c.m. system is decomposed:

$$u(p_1\lambda_1)=\frac{1}{[2m(E_1+m)]^{1/2}}\begin{bmatrix}E_1+m\\ k^*(-1)^{\lambda_1-\frac{1}{2}}\end{bmatrix}\chi_1(\lambda_1),\tag{B1}$$

where χ_1 is a spin eigenfunction referred to $\hat{p}_1=\hat{z}$ as a quantization axis.

In a similar fashion the Rarita-Schwinger spinor in the c.m. system is decomposed:

$$
\begin{aligned}
\bar{w}_\mu(p_2\lambda_2)=&\frac{1}{[2M(E_2+M)]^{1/2}}\sum_{\rho\sigma}(1\rho\tfrac{1}{2}\sigma|1\,\tfrac{1}{2}\,\tfrac{3}{2}\lambda_2)\chi_2{}^\dagger(\sigma)\\
&\times e_{2\nu}{}^\dagger(\rho)a_{\mu\nu}(-p_2)[E_2+M,\ -q^*(-1)^{\sigma-\frac{1}{2}}],
\end{aligned}
\tag{B2}
$$

where $\chi_2{}^\dagger$ and $e_{2\nu}{}^\dagger$ are spin-$\frac{1}{2}$ and spin-1 eigenstates referred to $\hat{p}_2$ as a quantization axis, and where $a_{\mu\nu}(-p_2)$ is the Lorentz transformation matrix

$$a_{\mu\nu}(-p_2)=\delta_{\mu\nu}+\frac{(p_{2\mu}+M\eta_\mu)(p_{2\nu}+M\eta_\nu)}{M(E_2+M)}-\frac{2p_{2\mu}\eta_\nu}{M}.\tag{B3}$$

Since $\eta_\mu=(0,0,0,i)$ in this frame and since $a_{\mu\nu}$ is always contracted in this frame with the purely spatial $e_{2\nu}{}^\dagger$, $a_{\mu\nu}(-p_2)$ may be written as

$$a_{\mu\nu}(-p_2)\doteq\delta_{\mu\nu}+[(p_{2\mu}+M\eta_\mu)/M(E_2+M)]p_{2\nu}.\tag{B4}$$

The angular momentum states with respect to the $\hat{p}_2$ axis (denoted by a subscript 2) may be expressed in terms of angular momentum states along $\hat{p}_1=\hat{z}$

(denoted by a subscript 1) by means of a rotation (see I):

$$\chi_2^\dagger(\sigma)=\sum_{\sigma'}\chi_1^\dagger(\sigma')\mathfrak{D}_{\sigma',\sigma}^{1/2*}(-\phi,-\theta,\phi),$$
$$e_{2\nu}^\dagger(\rho)=\sum_{\rho'}e_{1\nu}^\dagger(\rho')\mathfrak{D}_{\rho',\rho}^{1*}(-\phi,-\theta,\phi), \tag{B5}$$

where $e_{1\nu}(\pm1)=\mp(1/\sqrt{2})(1,\pm i,0,0)$ and $e_{1\nu}(0)=\hat{z}$.

Combining Eqs. (5.14)–(5.16) with (5.19) gives the general decomposition in the c.m. frame:

$$\langle\lambda_2|T^J(W,k^2)|\lambda_1\lambda_k\rangle$$
$$=+\frac{(4k^*q^*)^{1/2}}{8\pi W[(E_1+m)(E_2+M)]^{1/2}}\frac{1}{2}\int_{-1}^{1}d(\cos\theta)$$
$$\times\sum_{\rho\rho'\sigma\sigma'}(1\rho\tfrac{1}{2}\sigma|1\tfrac{1}{2}\tfrac{3}{2}\lambda_2)\mathfrak{D}_{\lambda_1-\lambda_k,\lambda_2}^{J}\mathfrak{D}_{\rho',\rho}^{1*}\mathfrak{D}_{\sigma',\sigma}^{1/2*}$$
$$\times a_{\mu\nu}(-p_2)e_{1\nu}^\dagger(\rho')\chi_1^\dagger(\sigma')[E_2+M,-q^*(-1)^{\sigma-1/2}]$$
$$\times\sum_{i=1}^{9}M_\mu^{(i)}(\lambda_k)A^{(i)}\begin{bmatrix}E_1+m\\k^*(-1)^{\lambda_1-1/2}\end{bmatrix}\chi_1(\lambda_1), \tag{B6}$$

where $\mathfrak{D}=\mathfrak{D}(-\phi,-\theta,\phi)$. For this calculation the Dirac matrix elements $\chi_1^\dagger[\cdots]M_\mu^{(i)}[\vdots]\chi_1$ were expanded by hand for each $M_\mu^{(i)}$, and then the angular integration was performed numerically using the $A^{(i)}$ in Appendix A.

APPENDIX C

Because coincidence experiments where the final electron and the final pion or proton are detected are necessary to separate the relative contribution of the multipole amplitudes in pion-electroproduction, and since experiments in the higher resonance region are now being considered,[45] the coincidence cross section is derived in this appendix. The coincidence cross section

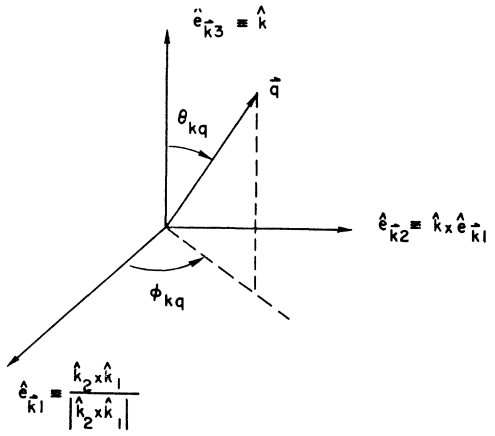

FIG. 14. Coordinate axes in the $|\pi N\rangle$ center-of-momentum frame.

[45] F. Pipkin (private communication).

for the $N^*(1236)$ was first analyzed by Berkelman,[46] and recently a general discussion has been given by Adler.[47] Because the result follows immediately from the analysis in I, the coincidence cross section is also presented here in the notation and variables of that paper. Equations (C26)–(C28) are also valid for $|\pi N^*(1236)\rangle$ coincidence measurements. Furthermore, the present discussion contains a detailed derivation of the basic noncoincidence cross section.

One starts from the expression for the S matrix:

$$S_{fi}=-(2\pi)^4i\delta^{(4)}(k_1+p_1-k_2-p_2-q)(m_e^2/\epsilon_1\epsilon_2\Omega^2)^{1/2}$$
$$\times(m^2/2\omega_qE_1E_2\Omega^3)^{1/2}T_{fi}, \tag{C1}$$
$$iT_{fi}=-4\pi\alpha[\bar{u}(k_2)\gamma_\mu u(k_1)/k^2](2\omega_qE_1E_2\Omega^3/m^2)^{1/2}$$
$$\times\langle qp_2{}^{(-)}|J_\mu|p_1\rangle \tag{C2}$$
$$iT_{fi}\equiv-4\pi\alpha\epsilon_\mu J_\mu. \tag{C3}$$

All the notation and conventions follow I. Note that T_{fi} is a Lorentz-invariant amplitude.

The laboratory cross section follows in standard fashion as

$$d\sigma_L=4(2\pi)^{-5}(d\mathbf{q}/2\omega_q)(d\mathbf{k}_2/2\epsilon_2)(d\mathbf{p}_2/2E_2)(m/\epsilon_1)$$
$$\times|m_eT_{fi}|^2\delta^{(4)}(k_1+p_1-k_2-p_2-q), \tag{C4}$$

where $d\sigma_L$ has been written in an explicitly Lorentz-invariant form ($\epsilon_1=-p_1\cdot k_1/m$). The resulting expression for $d\sigma_L$ can therefore be evaluated in any Lorentz frame.

The sum over electron spins can be carried out immediately. Defining

$$J_\mu\equiv(\mathbf{J},iJ_c), \tag{C5}$$
$$J_\mu^*\equiv(\mathbf{J}^*,iJ_c^*), \tag{C6}$$

one has

$$\tfrac{1}{2}m_e^2\sum_{s1}\sum_{s2}|J_\mu\epsilon_\mu|^2$$
$$=k^{-4}[(J\cdot k_1)(J^*\cdot k_1)+\tfrac{1}{4}k^2(J\cdot J^*)]. \tag{C7}$$

Now go the c.m. system for pion electroproduction. This frame is defined by

$$(p_1+k)_\mu=(\mathbf{0},iW). \tag{C8}$$

Defining a coordinate system as in Fig. 14 and using current conservation, one finds in the c.m. system

$$(J\cdot k_1)(J^*\cdot k_1)+\tfrac{1}{4}k^2(J\cdot J^*)_{\text{c.m. system}}$$
$$=|J_c|^2[((\mathbf{k}_1\cdot\hat{k})(k_0/k^*)-|\mathbf{k}_1|)^2-(k^4/4k^{*2})]$$
$$+\tfrac{1}{4}k^2|\mathbf{J}_\perp|^2+(\mathbf{k}_1\cdot\hat{e}_2)^2|\mathbf{J}\cdot\hat{e}_2|^2$$
$$+[(\mathbf{k}_1\cdot\hat{k})(k_0/k^*)-|\mathbf{k}_1|]$$
$$\times(\mathbf{k}_1\cdot\hat{e}_2)2\,\mathrm{Re}J_c^*(\mathbf{J}\cdot\hat{e}_2), \tag{C9}$$

[46] K. Berkelman, in *Proceedings of the International Symposium on Electron and Photon Interactions at High Energies, Hamburg, 1965* (Deutsche Physikalische Gesellschaft e.V., Hamburg, Germany, 1966), Vol. II, p. 299.

[47] Stephen L. Adler, Ann. Phys. (N. Y.) **50**, 189 (1968).

where

$$|\mathbf{J}_\perp|^2=|\mathbf{J}\cdot\hat{\epsilon}_1|^2+|\mathbf{J}\cdot\hat{\epsilon}_2|^2. \tag{C10}$$

The coefficients in this expression depending on the electron variables can be reexpressed in terms of laboratory variables ϵ_1, ϵ_2, and θ through the use of Eq. (C8). Thus, it follows that

$$\begin{aligned}(J\cdot k_1)(J^*\cdot k_1)+\tfrac{1}{4}k^2(J\cdot J^*)_{\text{c.m. system}}&\\ =(4\pi)^2\epsilon_1\epsilon_2\cos^2(\tfrac{1}{2}\theta)\{&(k^4/k^{*4})|\mathfrak{J}_c|^2+(W^2/m^2)\\ \times\tan^2(\tfrac{1}{2}\theta)\,&|\mathfrak{J}_1|^2+(k^2/k^{*2})|\mathfrak{J}\cdot\hat{\epsilon}_2|^2\\ -(k^2/k^{*2})[&(W^2/m^2)\tan^2(\tfrac{1}{2}\theta)+k^2/k^{*2}]^{1/2}\\ \times 2\,\mathrm{Re}\mathfrak{J}_c^*&(\mathfrak{J}\cdot\hat{\epsilon}_2)\},\end{aligned} \tag{C11}$$

where $\mathfrak{J}_\mu$ is defined by

$$\mathfrak{J}_\mu\equiv(m/4\pi W)J_\mu. \tag{C12}$$

Using the relation that in the c.m. system

$$\begin{aligned}(d\mathbf{q}/2\omega_q)(d\mathbf{p}_2/2E_2)\delta^{(4)}(k_1+p_1-k_2-p_2-q)&\\ =(q/4W)d\Omega_q^*,&\end{aligned} \tag{C13}$$

the cross section finally becomes

$$\begin{aligned}\frac{d^5\sigma_L}{d\epsilon_2 d\Omega_2 d\Omega_q^*/4\pi}=&\left[\frac{\alpha^2\cos^2(\tfrac{1}{2}\theta)}{\epsilon_1^2\sin^4(\tfrac{1}{2}\theta)}\right]\frac{mq}{W}\{(k^4/k^{*4})|\mathfrak{J}_c|^2\\ &+(k^2/k^{*2})|\mathfrak{J}\cdot\hat{\epsilon}_2|^2+(W^2/m^2)\tan^2(\tfrac{1}{2}\theta)|\mathfrak{J}_1|^2\\ &-(k^2/k^{*2})[(W^2/m^2)\tan^2(\tfrac{1}{2}\theta)+k^2/k^{*2}]^{1/2}\\ &\times 2\,\mathrm{Re}\mathfrak{J}_c^*(\mathfrak{J}\cdot\hat{\epsilon}_2)\}.\end{aligned} \tag{C14}$$

This fivefold cross section is a function of the five variables $(k^2,W^2,\theta,\theta_{kq},\phi_{kq})$, the first three being functions only of the laboratory electron variables ϵ_1, ϵ_2, and θ. Note also that the coordinate system in Fig. 14, and in particular the vector $\hat{e}_2$, is unchanged under the Lorentz transformation (along $\hat{k}$) from the laboratory to the c.m. system.

Equation (C14) gives the cross section for arbitrary initial and final nucleon spins. From I it follows that

$$\begin{aligned}\mathfrak{J}\cdot\hat{e}=\eta_{s_2}^\dagger[&i\boldsymbol{\sigma}\cdot\hat{e}\mathcal{F}_1+(\boldsymbol{\sigma}\cdot\hat{q})(\boldsymbol{\sigma}\cdot(\hat{k}\times\hat{e}))\mathcal{F}_2+i(\boldsymbol{\sigma}\cdot\hat{k})(\hat{q}\cdot\hat{e})\mathcal{F}_3\\ &+i(\boldsymbol{\sigma}\cdot\hat{q})(\hat{q}\cdot\hat{e})\mathcal{F}_4]\eta_{s_1},\end{aligned} \tag{C15}$$

$$\mathfrak{J}_c=\eta_{s_2}^\dagger[i\boldsymbol{\sigma}\cdot\hat{q}\mathcal{F}_7+i\boldsymbol{\sigma}\cdot\hat{k}\mathcal{F}_8]\eta_{s_1} \tag{C16}$$

for $\hat{e}\cdot\hat{k}=0$. The $\mathcal{F}_i$ are functions of k^2 and W. If the nucleon spins are not measured, one averages over initial spins and sums over final spins. Then

$$\tfrac{1}{2}\sum_{s_1}\sum_{s_2}|\mathfrak{J}_c|^2=|\mathcal{F}_7|^2+|\mathcal{F}_8|^2+2\,\mathrm{Re}\mathcal{F}_7^*\mathcal{F}_8\cos\theta_{kq}, \tag{C17}$$

$$\begin{aligned}\tfrac{1}{2}\sum_{s_1}\sum_{s_2}|\mathfrak{J}\cdot\hat{e}_2|^2=&|\mathcal{F}_1|^2+|\mathcal{F}_2|^2-2\,\mathrm{Re}\mathcal{F}_1^*\mathcal{F}_2\cos\theta_{kq}+\sin^2\theta_{kq}\sin^2\phi_{kq}\\ &\times(|\mathcal{F}_3|^2+|\mathcal{F}_4|^2+2\,\mathrm{Re}\mathcal{F}_1^*\mathcal{F}_4+2\,\mathrm{Re}\mathcal{F}_2^*\mathcal{F}_3+2\,\mathrm{Re}\mathcal{F}_3^*\mathcal{F}_4\cos\theta_{kq}),\end{aligned} \tag{C18}$$

$$\begin{aligned}\tfrac{1}{2}\sum_{s_1}\sum_{s_2}|\mathfrak{J}_1|^2=&2(|\mathcal{F}_1|^2+|\mathcal{F}_2|^2-2\,\mathrm{Re}\mathcal{F}_1^*\mathcal{F}_2\cos\theta_{kq})\\ &+\sin^2\theta_{kq}(|\mathcal{F}_3|^2+|\mathcal{F}_4|^2+2\,\mathrm{Re}\mathcal{F}_1^*\mathcal{F}_4+2\,\mathrm{Re}\mathcal{F}_2^*\mathcal{F}_3+2\,\mathrm{Re}\mathcal{F}_3^*\mathcal{F}_4\cos\theta_{kq}),\end{aligned} \tag{C19}$$

$$\begin{aligned}\tfrac{1}{2}\sum_{s_1}\sum_{s_2}2\,\mathrm{Re}\mathfrak{J}_c^*(\mathfrak{J}\cdot\hat{e}_2)=&\sin\theta_{kq}\sin\phi_{kq}[2\,\mathrm{Re}\mathcal{F}_1^*\mathcal{F}_7+2\,\mathrm{Re}\mathcal{F}_4^*\mathcal{F}_7+2\,\mathrm{Re}\mathcal{F}_2^*\mathcal{F}_8\\ &+2\,\mathrm{Re}\mathcal{F}_3^*\mathcal{F}_8+\cos\theta_{kq}(2\,\mathrm{Re}\mathcal{F}_3^*\mathcal{F}_7+2\,\mathrm{Re}\mathcal{F}_4^*\mathcal{F}_8)].\end{aligned} \tag{C20}$$

Equations (C14) and (C17)–(C20) give the final coincidence cross sections. Note that the angle ϕ_{kq} enters these expressions only through the combinations $\sin\theta_{kq}\sin\phi_{kq}$.[48]

These results can be written in a slightly different form by reintroducing the helicity amplitudes. Using

$$\begin{aligned}\hat{e}_{\pm1}&\equiv\mp\tfrac{1}{2}\sqrt{2}(\hat{e}_1\pm i\hat{e}_2),\\ \hat{e}_0&\equiv\hat{e}_3,\end{aligned} \tag{C21}$$

and defining

$$\mathfrak{J}^\lambda\equiv\mathfrak{J}\cdot\hat{e}_\lambda, \tag{C22}$$

one has

$$|\mathfrak{J}_1|^2=|\mathfrak{J}^{+1}|^2+|\mathfrak{J}^{-1}|^2, \tag{C23}$$

$$|\mathfrak{J}\cdot\hat{e}_2|^2=\tfrac{1}{2}|\mathfrak{J}_1|^2+\mathrm{Re}(\mathfrak{J}^{+1})^*(\mathfrak{J}^{-1}), \tag{C24}$$

$$2\,\mathrm{Re}\mathfrak{J}_c^*(\mathfrak{J}\cdot\hat{e}_2)=-\sqrt{2}\,\mathrm{Im}\mathfrak{J}_c^*(\mathfrak{J}^{+1}+\mathfrak{J}^{-1}). \tag{C25}$$

[48] The coordinate system shown in Fig. 14 differs from that defined by Adler (Ref. 47). The angle θ_{kq} is the same as his polar angle ϕ, but the angle ϕ_{kq} differs from his azimuthal angle δ by 90°. Thus $\theta_{kq}=\phi$, $\phi_{kq}=\delta+90°$. The definition of the isobaric frame amplitudes also differs from that chosen by Adler. The relation between the amplitudes is

$$\begin{aligned}\mathcal{F}_{1,2,3,4}&=(m/4\pi W)[\mathcal{F}_{1,2,3,4}{}^V]_{\text{Adler}},\\ \mathcal{F}_7&=(m/4\pi W)k^*[\mathcal{F}_6{}^V]_{\text{Adler}},\end{aligned}$$

and

$$\mathcal{F}_8=(m/4\pi W)k^*[\mathcal{F}_5{}^V]_{\text{Adler}}.$$

The cross section can therefore be written

$$\frac{d^5\sigma_L}{d\epsilon_2 d\Omega_2 d\Omega_q^*/4\pi}=\left[\frac{\alpha^2\cos^2(\frac{1}{2}\theta)}{\epsilon_1^2\sin^4(\frac{1}{2}\theta)}\right]\frac{mq}{W}\{(k^4/k^{*4})|\mathfrak{I}_c|^2$$
$$+[k^2/2k^{*2}+(W^2/m^2)\tan^2(\tfrac{1}{2}\theta)](|\mathfrak{I}^{+1}|^2+|\mathfrak{I}^{-1}|^2)$$
$$+(k^2/2k^{*2})2\,\mathrm{Re}(\mathfrak{I}^{+1})^*(\mathfrak{I}^{-1})+(k^2/k^{*2})$$
$$\times[(W^2/m^2)\tan^2(\tfrac{1}{2}\theta)+k^2/k^{*2}]^{1/2}\sqrt{2}$$
$$\times\mathrm{Im}\mathfrak{I}_c^*(\mathfrak{I}^{+1}+\mathfrak{I}^{-1})\}. \quad \text{(C26)}$$

Now from I,

$$\mathfrak{I}_{\lambda_2\lambda_1}^{\lambda_k}=(4k^*q)^{-1/2}\sum_J(2J+1)\mathfrak{D}_{\lambda_1-\lambda_k,\lambda_2}^{J}(-\phi_p-\theta_p\phi_p)^*$$
$$\times\langle\lambda_2|T^J(W,k^2)|\lambda_1\lambda_k\rangle, \quad \text{(C27)}$$

$$(\mathfrak{I}_c)_{\lambda_2\lambda_1}=(k^*/k_0)(4k^*q)^{-1/2}\sum_J(2J+1)$$
$$\times\mathfrak{D}_{\lambda_1\lambda_2}^{J}(-\phi_p-\theta_p\phi_p)^*\langle\lambda_2|T^J(W,k^2)|\lambda_1 0\rangle. \quad \text{(C28)}$$

The relation between the angles is obtained by comparing Fig. 4 of I with Fig. 14:

$$\theta_p=\theta_{kq}, \quad \phi_p=2\pi-\phi_{kq}. \quad \text{(C29)}$$

If only the electron is detected, one must integrate over the final pion direction, and using the orthogonality of the $\mathfrak{D}$ functions the interference terms in (C26) go out. Finally, summing and averaging over nucleon helicities gives

$$\tfrac{1}{2}\sum_{\lambda_1}\sum_{\lambda_2}\int\frac{d\Omega_q^*}{4\pi}|(\mathfrak{I}_c)_{\lambda_2\lambda_1}|^2$$
$$=\tfrac{1}{2}\sum_{\lambda_1}\sum_{\lambda_2}\left(\frac{k^*}{k_0}\right)^2(4k^*q)^{-1}\sum_J(2J+1)$$
$$\times|\langle\lambda_2|T^J(W,k^2)|\lambda_1 0\rangle|^2$$
$$=\sum_{J^\pi}(J+\tfrac{1}{2})|C_{l\pm}|^2, \quad \text{(C30)}$$

$$\tfrac{1}{2}\sum_{\lambda_1}\sum_{\lambda_2}\int\frac{d\Omega_q^*}{4\pi}[|\mathfrak{I}_{\lambda_2\lambda_1}^{+1}|^2+|\mathfrak{I}_{\lambda_2\lambda_1}^{-1}|^2]$$
$$=\tfrac{1}{2}\sum_{\lambda_1}\sum_{\lambda_2}(4k^*q)^{-1}\sum_J(2J+1)[|\langle\lambda_2|T^J(W,k^2)|\lambda_1 1\rangle|^2$$
$$+|\langle\lambda_2|T^J(W,k^2)|\lambda_1-1\rangle|^2]$$
$$=\sum_{J^\pi}(J+\tfrac{1}{2})[|T_{3/2}{}^{l\pm}|^2+|T_{1/2}{}^{l\pm}|^2], \quad \text{(C31)}$$

where the eigenstates of parity have been introduced. The resulting cross section for detection of only the electron is that given in Eq. (3.31) of I. The resonant amplitudes for producing the $|\pi N\rangle$ channel in the coupled-channel calculations are obtained by multiplying Eq. (5.31) by $\cos\varepsilon$.

PHYSICAL REVIEW VOLUME 184, NUMBER 5 25 AUGUST 1969

Anomalous Ward Identities in Spinor Field Theories

WILLIAM A. BARDEEN*†
Institute for Advanced Study, Princeton, New Jersey 08540
(Received 24 February 1969)

We consider the model of a spinor field with arbitrary internal degrees of freedom having arbitrary nonderivative coupling to external scalar, pseudoscalar, vector, and axial-vector fields. By carefully defining the S matrix in the interaction picture, the vector and axial-vector currents associated with the external vector and axial-vector fields are found to satisfy anomalous Ward identities. If we require that the vector currents satisfy the usual Ward identities, the divergence of the axial-vector current contains well-defined anomalous terms. These terms are explicitly calculated.

I. INTRODUCTION

THE presence of anomalous terms in the Ward identities for currents defined in a number of spinor field theories has been noted by several authors.[1–3] The existence of these terms may be traced to the local products of field operators which are so singular as to prohibit the naive use of the field equations. In a version of the σ model, the anomalous terms in the Ward identity for the neutral isospin current have led to a low-energy theorem for the decay $\pi^0\to\gamma\gamma$.[2]

In this paper, we consider a theory of a spinor field with an arbitrary number of internal degrees of freedom coupled to external scalar, pseudoscalar, vector, and

* Research sponsored by the Air Force Office of Scientific Research, U. S. Air Force, under AFOSR Grant No. 68-1365.
† Present address: Department of Physics, Stanford University, Stanford, California 94305.
[1] J. Steinberger, Phys. Rev. **76**, 1180 (1949); J. Schwinger, *ibid.* **82**, 664 (1951).
[2] S. L. Adler, Phys. Rev. **177**, 2426 (1969).
[3] C. R. Hagen, Phys. Rev. **176**, 2622 (1969); R. Jackiw and K. Johnson, *ibid.* **182**, 1457 (1969); R. Brandt, *ibid.* **180**, 1490 (1969); K. Wilson, *ibid.* **181**, 1909 (1969); J. S. Bell and R. Jackiw, Nuovo Cimento **60**, 47 (1969).